STUDY OF A NEW SOURCE FOR DUAL PHOTON ABSORPTIOMETRY OF THE LUMBAR SPINE

STUDY OF A NEW SOURCE FOR DUAL PHOTON ABSORPTIOMETRY OF THE LUMBAR SPINE

By

B.K. BHASKAR, B.TECH.

A Thesis

Submitted to the School of Graduate Studies

in Partial Fulfilment of the Requirements

for the Degree

Master of Engineering

McMaster University

April 1984

MASTER OF ENGINEERING (1984) McMASTER UNIVERSITY
Hamilton, Ontario

TITLE: Study of a New Source for Dual Photon Absorptiometry of the Lumbar Spine

AUTHOR: B.K. Bhaskar, B.Tech.

SUPERVISOR: Dr. Colin E. Webber, Ph.D. (Birmingham)

NUMBER OF PAGES: ix, 62

To my dear father

ABSTRACT

Bone disease and metabolic bone disorders are characterized by decrease in bone mineral content (BMC) and the vertebrae are primarily affected in osteoporosis. Thus it is essential to monitor changes in BMC due to disease, growth or therapy. Dual photon absorptiometry (DPA) is as yet the most efficient method for BMC determination in the lumbar vertebrae; most previous investigators have used ^{153}Gd which is generally accepted as possessing the ideal dual photon energy combination.

Davis and Webber (1978) developed a method for routine production of ^{153}Sm which emits photons of nearly the same energy as ^{153}Gd and suggested its use in DPA. In the present study using ^{153}Sm, measurements with aluminum standards immersed in water resulted in errors of 4% and 4.5% in accuracy and precision respectively for mass of Al in the range 0.4-1.8 $g.cm^{-2}$. These results were obtained using different volumes of water, verifying that bone mineral mass determined by this method is independent of soft tissue content. Experiments with bone mineral phantoms gave values which correlated highly (r=0.97) with results obtained on a commercially available clinical densitometer using ^{125}I.

Considering that these results are comparable with those obtained earlier using ^{153}Gd, that ^{153}Gd is scarcely available and several hundred times the cost, ^{153}Sm promises to be the potential source for routine clinical measurement of osteopenia in the lumbar spine by DPA. However, further invitro and invivo studies are necessary before it can be used regularly in nuclear medicine departments.

Acknowledgements

It is a pleasant duty to express my sincere gratitude to Dr. Colin E. Webber for having suggested this project and for his continued advice and encouragement throughout the course of this work. His cheerful guidance has been instrumental in the completion of this thesis.

I gratefully acknowledge the financial support received from McMaster University in the form of a scholarship and teaching assistantship and a scholarship from Dr. Ronald K. Ham Memorial Fund in the Department of Engineering Physics.

Special thanks are due to Dr. D.A. Thompson, Dr. W.v. Prestwich and Dr. J.W. Harvey for their encouragement and to Dr. T.J. Kennett for his invaluable suggestions in reviewing the text, especially in chapter 3.

I am also very thankful to Mrs. Kathy Noon for typing this thesis.

My heartfelt gratitude to my wife for her patience and understanding and to my brother for his encouragement.

The plotting of graphs were made possible through programs written by Dr.P.T.Wan and Mr.T.Beuthe.

Table of Contents

List of Figures

List of Tables

Nomenclature

I	Attenuated intensity of the higher energy photon
I_o	Unattenuated intensity of the higher energy photon
I'	Attenuated intensity of the lower energy photon
I'_o	Unattenuated intensity of the lower energy photon
m_a	Quantity of absorber a in gcm^{-2}
m_b	Quantity of absorber b in gcm^{-2}
N_i	True count rate, CPS
N_o	Observed count rate, CPS
x_d	Thickness of NaI(Tℓ) detector, cm
x_s	Radius of rod source, cm
x_{Al}	Thickness of aluminum window, cm
η	Absolute photopeak efficiency of the detector
τ	Deadtime of the system
μ_a	Attenuation coefficient of absorber a at the higher energy, cm^2g^{-1}
μ_b	Attenuation coefficient of absorber b at the higher energy, cm^2g^{-1}
μ'_a	Attenuation coefficient of absorber a at the lower energy, cm^2g^{-1}
μ'_b	Attenuation coefficient of absorber b at the lower energy, cm^2g^{-1}
μ_d	Linear attenuation coefficient of detector material, cm^{-1}
μ_s	Linear attenuation coefficient of acrylic, cm^{-1}
$\mu_{A\ell}$	Linear attenuation coefficient of aluminum, cm^{-1}

CHAPTER 1

Introduction

The technique of dual photon attenuation (DPA) has been developed and studied during the last fifteen years. The technique is an extension of the single photon method which is suitable for measuring bone mineral content (BMC) in the peripheral or appendicular bones of the body where a constant soft tissue thickness can be maintained (Fig. 1.1). In the single photon technique monoenergetic photons are attenuated through bone mineral and a uniform soft tissue mass; from the measured intensities through soft tissue and through bone, the mass of bone mineral in units of gcm^{-2} is determined using the exponential law of attenuation. The principle of the dual photon method is as follows: when photons at two different energies in a collimated beam are attenuated by bone mineral and non-uniform thicknesses of soft tissue, it is possible to separate the amounts of these substances due to the differential attenuation at the two photon energies by simultaneously solving the two exponential equations shown in Fig. 1.1. For stationary transmission measurements, this method will result in accurate values for the amount of bone mineral and soft tissue in the path of the photons in an ideal two compartment system. To determine the bone mineral content across a given area, a rectilinear scan procedure is followed with predetermined scan velocities and scan paths. However, corrections to both methods have to be made during in vivo measurements when varying quantities of fatty or adipose tissue are present constituting a three

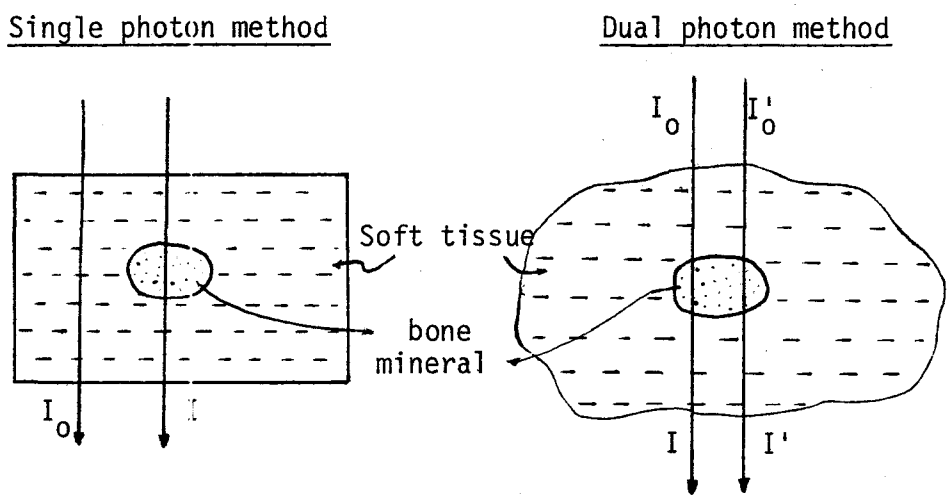

$$I = I_o e^{-\mu_a m_a}$$

$$I = I_o e^{-\mu_a m_a - \mu_b m_b}$$

$$I' = I'_o e^{-\mu'_a m_a - \mu'_b m_b}$$

Fig. 1.1: Sketch of single and dual photon methods.

compartment system. In both methods, the transmitted photons are detected by a collimated NaI (Tℓ) detector located at a constant distance from the source.

Generally clinical requirements are for mineral measurements in the central or axial skeleton where bone fractures occur. Unfortunately at such sites constant soft tissue thickness cannot be provided. In these circumstances the dual photon technique is imperative. Its usefulness in the determination of bone mineral content for clinical applications has been well established. Bone disease and metabolic bone disorders are characterized by decrease in BMC [1] and a concurrent loss of bone strength. A high correlation was observed between mineral content and crushing stress at elastic limit in lumbar vertebrae [2]. Krolner and Nielsen [3] have shown in their cross-sectional and longitudinal studies that measurement of lumbar BMC is useful for the diagnosis of spinal osteoporosis. The vertebrae are primarily affected in senile osteoporosis [4] leading to vertebral fractures and hence measurement of spinal BMC is important for diagnosis of osteoporosis.

Most investigators used either the isotope ^{153}Gd (photons at 44 kev and 100 kev) or combinations of two isotopes such as ^{241}Am (59.6 kev) and ^{137}Cs (662 kev) as sources for photons of two different energies. The application of dual photon absorptiometry was first suggested in 1963 by Cameron and Sorenson [5] using the radioactive isotopes ^{125}I and ^{241}Am for the determination of BMC in the forearm. They reported an average accuracy of 3% when the quantity of $CaCO_3$ present in mixtures of $CaCO_3$ and paraffin was measured. Reed [6]

described the use of the dual sources ^{241}Am and ^{137}Cs to determine calcium in bone and to study bone mineralization. Roos et al [7] utilized the same isotope pair in a scanning procedure for measuring bone mineral in the vertebrae. The dual photon technique was also developed by Mazess et al [8] with the radioisotope ^{153}Gd which has photon emissions around 44 kev and 100 kev.

Hanson [9] modeled the precision of the dual attenuation technique by an expression for the coefficient of variation of bone mineral measurement, to compare the dual photon sources ^{153}Gd and ^{125}I, ^{241}Am. His results showed that for the ratio of bone mineral mass to soft tissue mass of 0.2, ^{153}Gd was more precise for thick body sections (where bone mineral >1.2 gcm^{-2}) and ^{125}I, ^{241}Am was more precise for thin sections (where bone mineral <1.2 gcm^{-2}). In another theoretical analysis, Watt [10] evaluated the minimum Relative Error Function (defined as a direct proportion of the coefficient of variation of bone mineral) to determine the optimum energy combination for different absorber thicknesses and bone mineral fractions. With 15.0 gcm^{-2} total absorber thickness and 0.1 fraction by weight of bone mineral, he obtained the optimum energies for maximum precision to be 40 kev and 400 kev in the dual photon method. Smith et al [11] compared the sources ^{153}Gd and ^{241}Am, ^{137}Cs for soft tissue thickness of 5 gcm^{-2} to 30 gcm^{-2} and bone mineral content of 0.6 gcm^{-2} to 1.4 gcm^{-2} which are typically present in normal adults. By minimizing the Comparative Error Function (CEF) which is similar to the REF defined by Watt [10], they found the optimum energy combination to be 43 kev and 180 kev for a bone mineral of 1.0 gcm^{-2} and soft tissue thickness of 20 gcm^{-2}.

Their results showed that the upper energy level had little effect on CEF and that ^{153}Gd was superior to ^{241}Am, ^{137}Cs which also gave clinically viable results. However, they argued that in view of the irregular availability and greater cost of ^{153}Gd, the dual source ^{241}Am, ^{137}Cs was a practical alternative for spine BMC measurements.

In order to evaluate changes in BMC in the lumbar spine due to disease, growth or therapy, a high accuracy and precision in the measurements is essential. In studies with ^{153}Gd, Mazess et al [12] obtained an accuracy below 2% with dipotassium hydrogen phosphate standards immersed in water. They found the BMC in normal persons to be uniform along the spine within 3% and in osteoporosis they observed about 70% mineral loss in specific areas of the spine. Wilson and Madsen [13] reported a correlation coefficient of 0.99 in measurements using dipotassium hydrogen phosphate phantoms to simulate spinal bone tissue. Dunn et al [14] also obtained a correlation coefficient of 0.99 between actual and measured mass of ashed bone samples immersed in water and oil. Krolner and Nielsen [15] developed a scanning technique using ^{153}Gd and achieved invitro accuracy of 1.3% in measurements with bone mineral equivalent solutions.

As indicated by Smith et al [11], for clinical studies of metabolic disorders of bone, the precision of the dual photon method should be around 2%. Kan et al [16] developed an analog device for direct readout of BMC and bone width from dichromatic absorptiometry using ^{153}Gd and obtained a precision below 2% on human upper arm measurements. Roos and Skoldborn [17] utilized the dual source ^{241}Am, ^{137}Cs in

their experiments with patients and phantoms. They obtained a precision of 3% in measurements with phantoms and 3-8% in measurement of the lumbar spine BMC in patients. Corrections for the presence of adipose tissue were made by baseline adjustment of the transmission curve. In studies with ^{153}Gd, Mazess et al [12] reported a precision of 3% for the BMC of the lumbar spine in normal subjects measured over a one month period. In measurements with dipotassium hydrogen phosphate phantoms, Wilson and Madsen [13] obtained a precision of 1.7% and in measurements on four individuals the precision ranged from 0.7-3.8%. Condon et al [18] used the dual sources ^{241}Am, ^{137}Cs in measuring bone mineral in the 2nd, 3rd and 4th lumbar vertebrae and obtained long-term reproducibility of 2% on phantoms and 3% on patients. Krolner and Nielsen [15] achieved in vitro precision of 0.9-2.3% in measurements with bone mineral standards and human lumbar vertebrae over a six month period. The invivo precision in measurements on ten subjects varied from 1.4-2.6%. In another study using ^{153}Gd, Dunn et al [14] reported a precision of 1.8% with bone mineral phantoms and 1.3% for lumbar spine measurements in five volunteers. Tothill et al [19] compared the sources ^{153}Gd and ^{241}Am, ^{137}Cs for the measurement of BMC in the lumbar spine by DPA and concluded that ^{153}Gd was superior with a precision of 1-3% in subject measurements. Riggs et al [20] used the isotope ^{153}Gd and obtained a precision of 2.3% in lumbar spine measurements on five volunteers during a ten month period. They showed that spinal osteoporosis was characterized better by the vertebral bone mineral density rather than the presence of nontraumatic vertebral fractures and they defined a value of 0.965 gcm^{-2} as a threshold below which the

risk for vertebral fracture increased. Their results proved that direct measurements of bone density was essential to assess spinal osteoporosis. Smith et al [11] obtained a precision of 1.1-2.5% with an anthropomorphic phantom using ^{153}Gd and with a wax phantom their precision was 0.6% using ^{241}Am, ^{137}Cs and 0.4% using ^{153}Gd. The precision of fat estimation with 20 gcm^{-2} soft tissue and 15% fat was 1.7% using ^{153}Gd and 3.8% using ^{241}Am, ^{137}Cs.

The isotope ^{153}Sm emits photons of nearly the same energy as ^{153}Gd. Davis and Webber [21] developed a method for routine production of ^{153}Sm in a reactor, showing it to be economical and more easily available than ^{153}Gd and suggested that ^{153}Sm could replace ^{153}Gd in all applications where it has hitherto been used, including dual photon absorptiometry.

^{153}Gd has a half-life of 242d and has to be replaced annually. ^{153}Sm has a half-life of 46.8h and needs to be replaced every week. As shown by Smith et al [11], a high activity ^{153}Gd source could be used for two years provided the source collimator dimensions were changed to avoid deadtime errors at high activity and to obtain a high enough count rate at low activity. The disadvantage of this will be the change in geometry with a possible introduction of errors into BMC measurements. Ideally, longitudinal studies spanning several years necessitate absolutely reproducible parameters for useful results. This would be possible with weekly production of ^{153}Sm.

The purpose of this preliminary investigation is to study the radioisotope ^{153}Sm and to evaluate and assess its usefulness in DPA of the lumbar vertebrae.

CHAPTER 2

Efficiency Calibration of a Thin NaI(Tℓ) Crystal Detector

2.1 Introduction

The objective of the undermentioned measurements is to determine the absolute intensities of the two groups of photons emitted from the radioisotope source (^{153}Sm) to be used for In-Vivo dual photon transmission measurements of the mineral content of the lumbar spine. ^{153}Sm is produced in the McMaster University nuclear reactor by thermal neutron activation of enriched ^{152}Sm. Following the negatron beta decay of ^{153}Sm, the predominant emissions are 103 kev gamma rays and Eu K-xrays (≃42.5 kev) due to internal conversion. To fully understand the relation between transmission of photons through an object and the elemental composition of the object, it is necessary to know the incident flux at each photon energy. The incident flux for a given source will be determined by the inherent decay characteristics of ^{153}Sm and the self-absorption of photons by the source. A series of measurements were designed using a NaI(Tℓ) detector to measure the absolute intensities of the major photon emissions of ^{153}Sm and to assess the self-absorption in a number of reactor produced ^{153}Sm sources.

The absolute photopeak efficiency of a scintillation detector is defined as the ratio of the number of gamma rays totally absorbed in the crystal to the number of source gamma rays emitted within the solid angle subtended by the detector at the source. The number of gamma rays totally absorbed in the crystal is given by the photopeak area

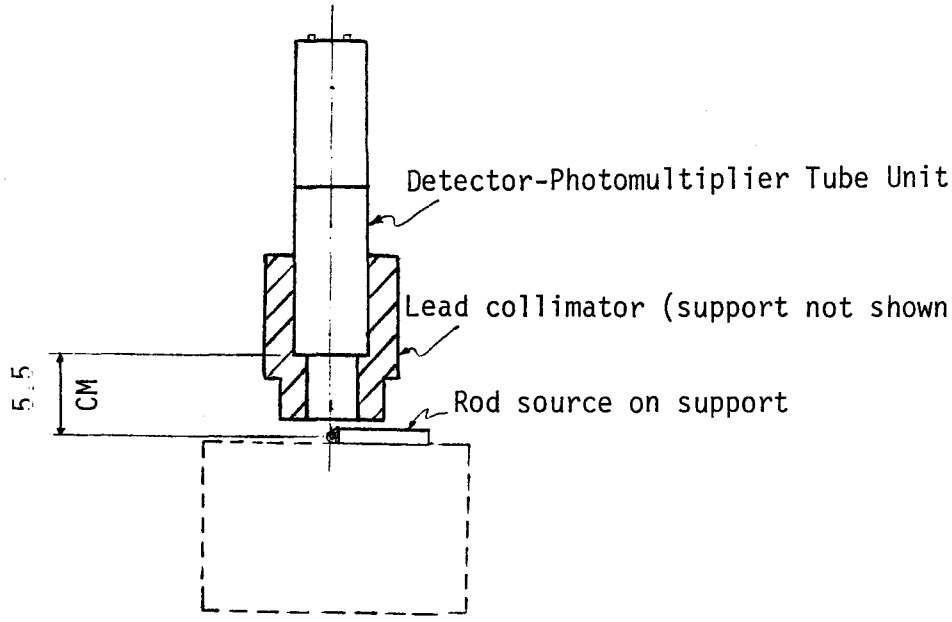

Fig. 2.1: Source-detector arrangement.

of the pulse height spectrum obtained on a multichannel analyzer (canberra series 30). The energy range of concern is 10 kev to 130 kev. The detector system consists of a 5.08cm Dia. x 0.3175 cm thick NaI(Tℓ) crystal with a 0.0254 cm thick aluminum window and a lead collimator 2.54cm I.D. x 5.0 cm long. Standard rod sources of ^{57}Co, ^{109}Cd, ^{133}Ba and ^{241}Am were used with source to detector distance 5.5 cm in all cases (Fig. 2.1).

2.2 Theoretical Evaluation

The efficiency values for different energies were calculated using the following expression [22]:

$$\eta = [1 - \exp(-\mu_d x_d)].\exp(-\mu_s x_s).\exp(-\mu_{A\ell} x_{A\ell})$$

where η is the absolute photopeak efficiency; μ_d, μ_s, $\mu_{A\ell}$ are the total absorption coefficients of the detector material (NaI(Tℓ)), intermediate source attenuating material (Acrylic) and of aluminum respectively; x_d, x_s and $x_{A\ell}$ are the path lengths of the gamma rays through the three corresponding materials. Self absorption in the rod sources ($e^{-\mu_s x_s}$) was considered since the relative absorption at low energies is high. The values of the absorption coefficients used were taken from the tables of Storm and Israel [23]. Since these were given for 10 kev intervals it was important to fit the data to an expression to allow the interpolation of coefficients at intermediate energies. Various polynomial fits of different degrees (using the International Mathematics and Statistics Libraries (IMSL) subroutine RLFOR) failed to give accurate expressions for absorption coefficients of Na, I and Aℓ.

The best polynomial fits across the energy range 10-150 kev yielded for the percentage of variation of the estimated models, values as large as 30%. The data were then grouped into energy regions based on the linearity observed over different portions of a log-log plot of absorption coefficients and energy. A general expression of the form

$$\ell n\mu = A\ \ell nE + B$$

where μ is in $cm^2\ g^{-1}$, E is in kev and A and B are constants, was fitted to the data for each energy region. The constants were determined using IMSL subroutine RLONE. The results are given in Table 2.1.

For each element, the value at 122.1 kev was obtained by linear interpolation. Densities of 2.694 gcm^{-3} for Aℓ and 3.67 gcm^{-3} for NaI were used. To estimate self-absorption in the rod source, the data given by the manufacturer (New England Nuclear) was used; that is a rod diameter of 1.27 cm and composition of acrylic as 60.04% carbon, 7.97% Hydrogen, 31.99% oxygen with a density of 1.185 gcm^{-3}. As before, the total absorption coefficients of C, H and O were obtained from [23] and fitted as shown in Table 2.1. In each case, the values at energies outside the indicated energy ranges were obtained by linear interpolation. The total absorption coefficients used are shown in Table 2.2 along with the computed efficiencies. A maximum error of 10% is quoted in [23] for the total absorption coefficients. Tables of these values in [24] report an accuracy of 1% to 2% and [25] gives polynomial fits for these values with an error of 1%. Using [25], the total absorption coefficients of NaI(Tℓ) are computed with a maximum error of 3% and are also shown in Table 2.2 along with the calculated efficiencies.

ELEMENT	ENERGY REGION (KeV)	A	B	CORR. COEFF.
I	8 - 33.17	- 2.73	11.31	1.00
	33.17 - 100	- 2.04	9.81	0.99
Na	10 - 50	- 3.09	9.79	1.00
	50 - 100	- 1.87	4.99	0.99
Al	10 - 100	- 2.91	9.82	1.00
C	10 - 50	- 2.82	7.02	0.99
H	10 - 50	0.66	- 6.23	0.99
O	10 - 60	- 2.93	8.30	0.99

TABLE 2.1 - Parameters for computing absorption coefficients

ENERGY (KeV)	μ_{NaI} (cm^{-1})	μ_{Al} (cm^{-1})	$\mu_{Acrylic}$ (cm^{-1})	Efficiency (using (23))	μ_{NaI} (cm^{-1} from (25))	Efficiency (using (25))
14.4	177.49	21.15	1.06	0.31	199.60	0.31
22.2	55.70	6.16	0.31	0.71	63.13	0.71
31.0	21.81	2.27	0.12	0.88	21.71	0.88
59.6	13.34	0.34	0.03	0.96	24.20	0.97
81.0	7.13	0.14	0.03	0.88	10.90	0.95
88.0	6.02	0.11	0.03	0.84	8.46	0.91
122.1	3.09	0.09	0.03	0.61	4.00	0.70

TABLE 2.2 - Theoretical Efficiency at Different Energies

At very low energies (<25 kev), absorption in the Aℓ window and self-absorption in the rod source is high, resulting in low detection efficiencies. As the photon energy increases, this absorption decreases. At the same time absorption in NaI increases rapidly with an increase in detection efficiency. At even higher energies (>60 kev), absorption in NaI decreases, there is little source self-absorption and absorption in the Aℓ window, leading to lower efficiencies.

2.3 Experimental Determination

The detector is a crystal-photomultiplier integral unit (ser. # HN708174) and was supported with its axis vertical. The photomultiplier tube preamplifer was connected through a DDL Amp. (Canberra Model 1411) to the MCA. A reference pulser (Canberra Model 1407) was also coupled to the input of the amplifier. The pulse amplitude was adjusted so that the pulser peak was located on the MCA display beyond the pulse height spectra of the rod sources. The pulser was necessary to correct for counting losses which occurred despite deadtime corrections in the timer setting of the MCA. In each case background counts were subtracted. The various gamma ray intensities and the isotope half lives are given in Table 2.3. Since no unified reference is available for these isotopes, it was necessary to use the results of different investigators to compile the data shown in Table 2.3.

Three measurements of detector efficiency were made over a period of four days for each rod source positioned 5.5 cm from the detector face. The results are shown in Table 2.4. Corrections were made for the presence of associated photons in the photopeaks listed

ISOTOPE	ENERGY (KeV)	INTENSITY (%)	HALF-LIFE	REFERENCE
^{57}Co	14.4 122.1	9.38 85.3	270d	(26), (27)
^{109}Cd	22.2 88.0	85.3 3.79	453d	(28)
^{133}Ba	31.0 81.0	95.1 34.7	10.7^{4}y	(29)
^{241}Am	59.6	36.0	458y	(26)

TABLE 2.3 - Intensity and Half-life data for the radioisotopes used

TABLE 2.4 - Measured efficiencies at various photon energies

ENERGY (KeV)	CPS FROM SPECTRUM AFTER CORRECTION	UNATTENUATED SOURCE ACTIVITY PHOTON/SEC	EFFICIENCY	AV. EFFICIENCY
14.4	29.34	1.52×10^4	$0.27 \pm .02$	$0.27 \pm .02$
	28.47	1.51×10^4	$0.27 \pm .02$	
	28.03	1.50×10^4	$0.26 \pm .02$	
22.2	1762.12	24.98×10^4	$0.64 \pm .04$	$0.63 \pm .04$
	1714.36	24.90×10^4	$0.62 \pm .04$	
	1692.34	24.86×10^4	$0.62 \pm .04$	
31.0	19.56	0.19×10^4	$0.83 \pm .06$	$0.84 \pm .06$
	20.03	0.19×10^4	$0.85 \pm .06$	
	19.80	0.19×10^4	$0.84 \pm .06$	
59.6	867.20	6.98×10^4	$0.92 \pm .06$	$0.92 \pm .06$
	884.50	6.98×10^4	$0.93 \pm .06$	
	849.33	6.98×10^4	$0.90 \pm .06$	
81.0	7.89	0.07×10^4	$0.87 \pm .06$	$0.87 \pm .06$
	7.98	0.07×10^4	$0.88 \pm .06$	
	7.88	0.07×10^4	$0.87 \pm .06$	
88.0	118.89	1.11×10^4	$0.82 \pm .06$	$0.82 \pm .06$
	121.57	1.11×10^4	$0.83 \pm .06$	
	119.29	1.10×10^4	$0.82 \pm .06$	
122.1	987.44	13.79×10^4	$0.55 \pm .04$	$0.55 \pm .04$
	1027.69	13.72×10^4	$0.57 \pm .04$	
	963.13	13.69×10^4	$0.54 \pm .04$	

in Table 2.3. These were for ^{109}Cd the 25 kev k_β x-rays, for ^{133}Ba the 35 kev k_β x-rays and the 79.6 kev gamma rays and for ^{57}Co the 136.5 kev gamma rays. Intensities of these associated photons were also obtained from the corresponding references listed in Table 2.3. No corrections were made for photon backscattering or for scattering from the collimator, because the measurement geometry made backscattering unlikely and scattering from a lead collimator is not favoured for low energy photons. In order to measure iodine escape, a 2 mm thick Cu absorber was placed between the rod source and detector in order to totally absorb the lower energy source emissions (<45 kev). An iodine escape peak, of 15.5%, was observed only for the ^{241}Am source and correction due to this was made for the 59.6 kev measurement. The absence of prominent iodine escape peaks for the 81, 88 and 122.1 kev photons is possibly due to the rapid increase of mean free path for increasing energies (0.4 mm for 59.6 kev, 0.9 mm for 81 kev, 1.2 mm for 88 kev and 2.5 mm for 122.1 kev) and also due to low energy resolution of the detector at these energies. Finally, for isotopes with emissions at two energies, measurements were made with the same cu absorber as before. The contribution of the 88 kev photons to the 22.2 kev energy window in the MCA was found to be 3.8%, contribution of the 81 kev photons to the 31 kev window was 16% and that due to 122.1 kev photons to the 14.4 kev window was 0.5%; accordingly, corrections were made for the lower energy measurements.

2.4 Conclusions

The theoretical and experimental values of efficiency are com-

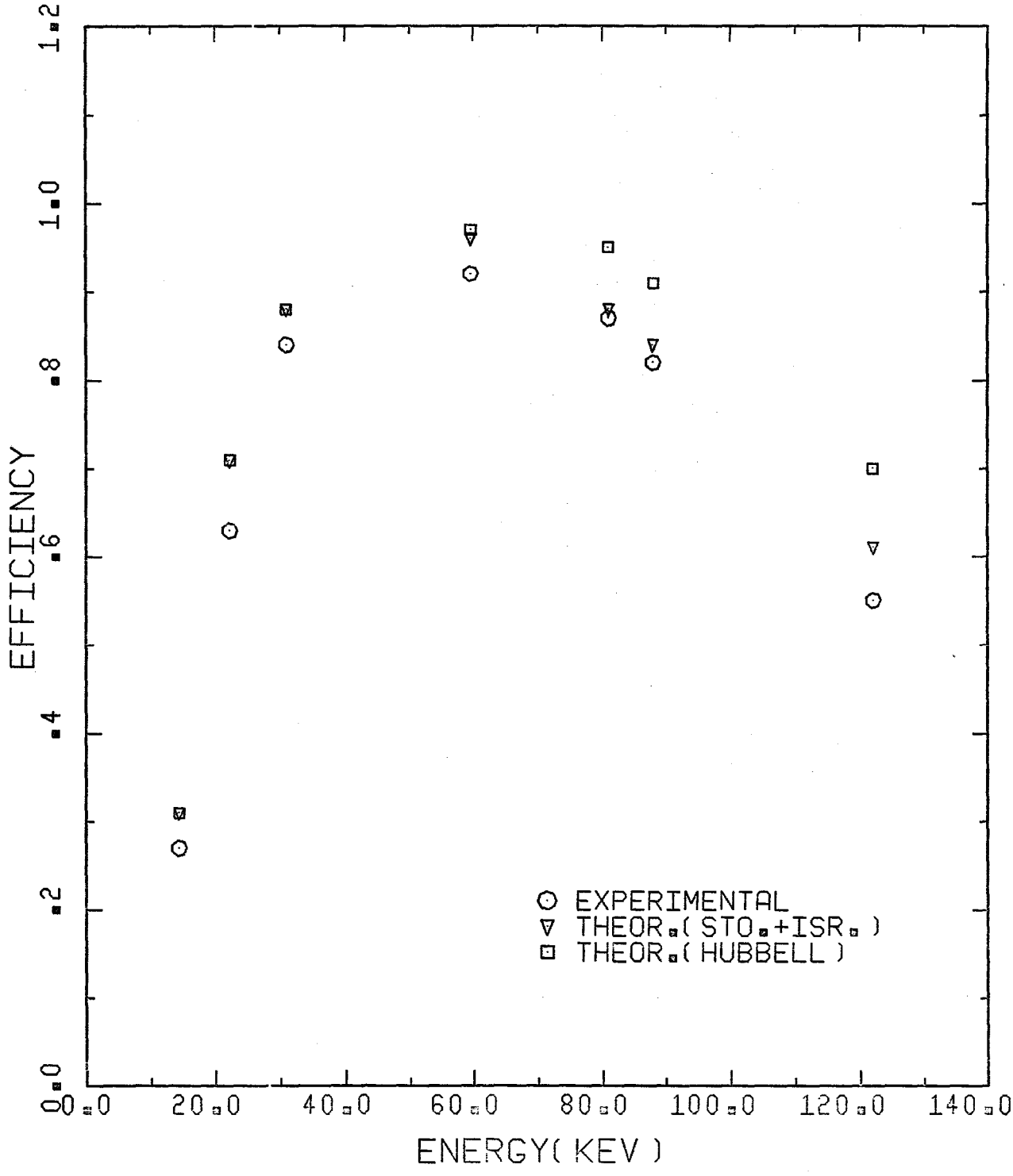

Fig. 2.2: Plots of efficiency vs. energy.

pared in Fig. 2.2 and a good correspondence is observed. The typical error due to counting statistics in the measurements is 1%. The accuracy of the source activities is 5%. Errors arising from variations in positioning of the rod source and from the corrections mentioned earlier, mean that the overall error in the results may be 7%. From these results it is concluded that the detector efficiencies for the 103 kev and 42.5 kev photons of ^{153}Sm are 0.71 and 0.90 respectively.

CHAPTER 3

Count Rate Characteristics

In this chapter the following five characteristics of the source-detector combination are discussed: the nature of the relation between water thickness and attenuation of the 42.5 and 103 kev photons; dead-time effects; photon absorption in the source material; source activity as a function of detector count rate and finally the geometry of the photon beam.

3.1 Exponential Attenuation

The technique of DPA is applicable to photon intensities following the exponential law of attenuation. This has been investigated for a range of water thicknesses from 5 cm to 25 cm, for the 42.5 kev and 103 kev photons of ^{153}Sm.

Measured quantities ($\sim$26 mg) of $^{152}Sm_2O_3$ (98.29%) were inserted into specially constructed graphite capsules shown in fig. 3.1. These capsules were irradiated in the McMaster Nuclear Reactor for a few hours to obtain ^{153}Sm. The collimated source holder was located on a modified OHIO Nuclear Rectilinear scanner and the NaI(Tℓ) detector aligned at a distance of about 50 cm from the source. Known volumes of water were taken in a graduated glass cylinder to obtain different thicknesses. Counts in the 42.5 kev and 103 kev photopeaks were registered in the MCA and the contribution from the higher energy to the lower energy region was determined using 4 mm thick copper sheets to absorb the low energy photons. Windows were set to include the total photopeaks in

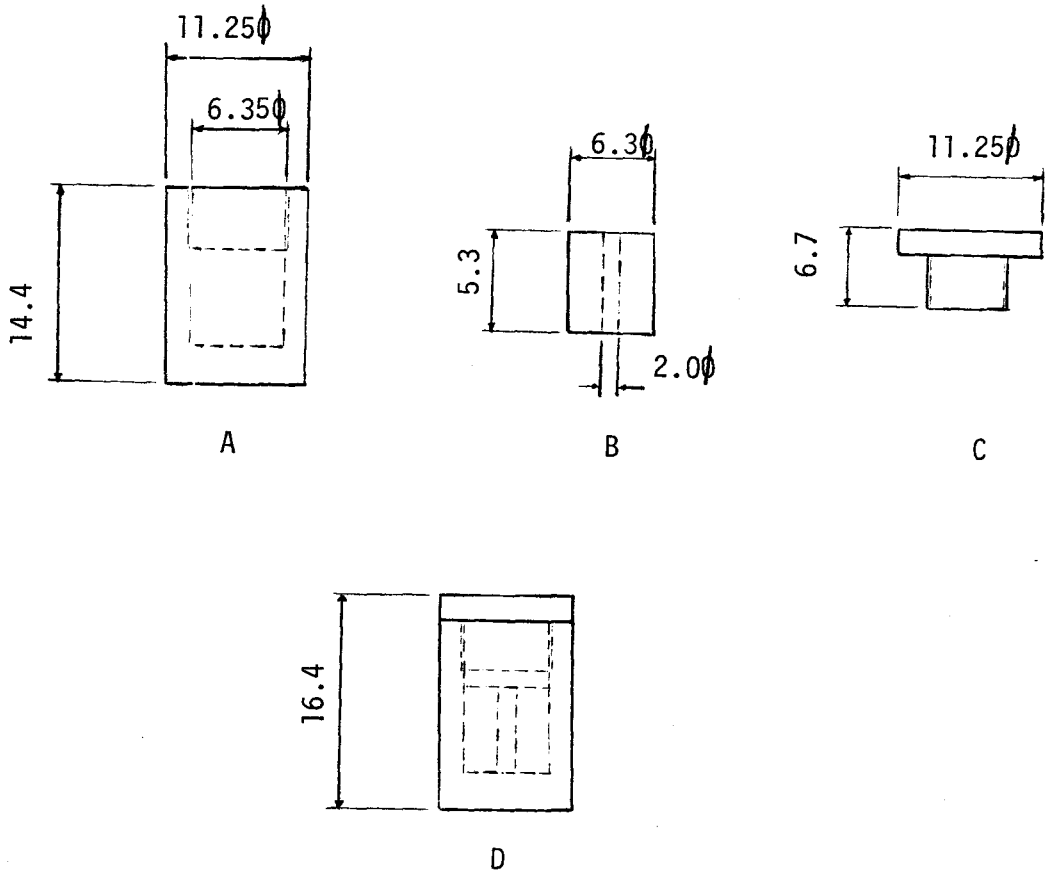

All dimensions in MM

A Graphite capsule

B Cylindrical graphite insert with central hole

C Threaded graphite cap

D Assembled source capsule

Fig. 3.1: Graphite capsule for ^{153}Sm source

both the energy channels. The compton contribution to the lower energy channel was found to be 7% of total counts under the higher energy peak. This was obtained from measurements with different ^{153}Sm sources and different water thicknesses. The variation was less than 1% showing it to be independent of water thickness. Tables 3.1A, 3.1B and 3.1C indicate for three separate experiments each performed with the same source, the measured count rates for different water thicknesses along with the corrected true count rates. The MCA counts were corrected for decay and as before, a pulser was used concurrently to obtain the true counts. A logarithmic fit using RLONE yielded for the measurements in each experiment, the corresponding exponential equations shown in Table 3.1 for the 42.5 kev and 103 kev photons. The derived attenuation coefficients for water are also indicated in these tables and the mean values are 0.246 ± .007 cm^{-1} at 42.5 kev and 0.170 ± .005 cm^{-1} at 103 kev. By fitting the data of Hubbell (1969) for the total attenuation coefficient for water, the values of 0.255 cm^{-1} and 0.169 cm^{-1} were obtained at 42.5 kev and 103 kev respectively. The error reported by Hubbell is 1-2% in his attenuation data and the error in the derived data is 3%. The above results verify that these photon intensities obey the exponential law of attenuation.

3.2 Deadtime

Another common source of error in count rate measurements is due to the deadtime of the system. In this respect two types of deadtimes are recognized - paralyzable and nonparalyzable. The type of response depends on whether or not the deadtime of the system is

WATER THK. cm, x	COUNT TIME SEC.	PULSER COUNTS		OBS. CPS. w/ DECAY CORR.		TRUE CPS, N	
		TRUE	OBS.	42.5 KeV	103 KeV	42.5 Kev	103 KeV
2.55	10	600	566	3577.4	4247.7	3792.3	4502.9
3.82	10	600	582	2607.2	3476.6	2687.8	3584.1
5.10	10	600	595	1934.9	2675.8	1951.2	2698.3
6.37	20	1200	1196	1396.8	2160.5	1401.5	2167.7
7.65	20	1200	1185	1026.7	1774.4	1039.7	1796.9
8.92	20	1200	1174	718.2	1438.1	734.1	1469.9
10.20	30	1800	1796	548.5	1173.7	549.7	1176.3
11.47	30	1800	1787	394.1	937.4	396.9	944.2
12.75	50	3000	2979	283.0	759.1	285.0	764.4
14.02	50	3000	2983	201.2	609.1	202.3	612.6
15.30	90	5400	5376	151.1	486.4	151.8	488.6
16.57	90	5400	5369	112.3	400.1	112.9	402.4
17.85	90	5400	5374	75.1	317.5	75.5	319.0
19.12	200	12000	11987	55.6	252.9	55.7	253.2
20.40	200	12000	11984	42.0	208.4	42.1	208.7
21.67	200	12000	11997	30.2	165.4	30.2	165.4
22.95	300	18000	17998	22.3	135.2	22.3	135.2
24.22	400	24000	23997	17.2	107.2	17.2	107.2
25.50	500	30000	29996	12.8	89.8	12.8	89.8

$\mu_{42.5} = 0.250 \pm .007$ cm^{-1}; $\mu_{103} = 0.170 \pm .005$ cm^{-1}

for 42.5 KeV: $N = 6925.2e^{-.250x}$

for 103 KeV: $N = 6658.4e^{-.170x}$

TABLE 3.1A - Attenuation coefficient for water -1

WATER THK. cm, x	COUNT TIME SEC.	PULSER COUNTS		OBS. CPS. w/DECAY CORR.		TRUE CPS, N	
		TRUE	OBS.	42.5 KeV	103 KeV	42.5 KeV	103 KeV
2.55	20	1200	1193	1269.1	1946.9	1276.5	1958.3
3.82	20	1200	1192	890.4	1524.9	896.4	1535.1
5.1	20	1200	1196	631.3	1228.8	633.4	1232.9
6.37	20	1200	1194	452.7	990.8	454.9	995.8
7.65	30	1800	1792	343.7	802.2	345.2	805.8
8.92	30	1800	1789	238.6	636.0	240.1	639.9
10.2	40	2400	2380	174.2	519.5	175.7	523.9
11.47	60	3600	3589	127.6	417.4	128.0	418.7
12.75	60	3600	3592	93.3	336.4	93.5	337.1
14.02	80	4800	4798	68.3	268.9	68.3	269.0
15.3	80	4800	4789	52.0	227.4	52.1	227.9
16.57	100	6000	5999	36.4	178.3	36.4	178.3
17.85	200	12000	11998	25.7	143.9	25.7	143.9
19.12	300	18000	17996	21.1	117.5	21.1	117.5
20.4	300	18000	17998	15.1	93.4	15.1	93.4
21.67	400	24000	23998	11.7	76.2	11.7	76.2
22.95	500	30000	29997	8.1	61.6	8.1	61.6
24.22	500	30000	29999	6.7	50.4	6.7	50.4
25.5	600	36000	35996	4.8	40.4	4.8	40.4

$\mu_{42.5} = 0.242 \pm .007\ cm^{-1}$; $\mu_{103} = 0.168 \pm .005\ cm^{-1}$

for 42.5 KeV: $N = 2148.1e^{-.242x}$

for 103 KeV: $N = 2913.1e^{-.168x}$

TABLE 3.1B - Attenuation coefficient for water -2

WATER THK. cm,x	COUNT TIME SEC.	PULSER COUNTS		OBS. CPS. w/DECAY COR.		TRUE CPS,N	
		TRUE	OBS.	42.5 KeV	103 KeV	42.5 KeV	103 KeV
5.1	10	600	540	6740.0	7401.4	7488.9	8223.8
7.65	10	600	593	3683.0	5406.8	3726.5	5470.6
10.2	10	600	586	1938.3	3189.5	1984.6	3265.7
12.75	10	600	583	963.6	2126.0	991.7	2188.0
15.3	20	1200	1192	540.4	1465.8	544.0	1475.6
17.85	20	1200	1180	310.2	917.9	315.4	933.4
20.4	40	2400	2363	167.6	557.1	170.2	565.8
22.95	60	3600	3565	95.2	357.5	96.1	361.0
25.5	90	5400	5352	42.0	269.5	42.4	271.9

$\mu_{42.5} = 0.247 \pm .007\ cm^{-1}$; $\mu_{103} = 0.171 \pm .005\ cm^{-1}$

for 42.5 KeV: $N = 24873.8e^{-.247x}$

for 103 KeV: $N = 19507.9e^{-.171x}$

TABLE 3.1C - Attenuation coefficient for water -3

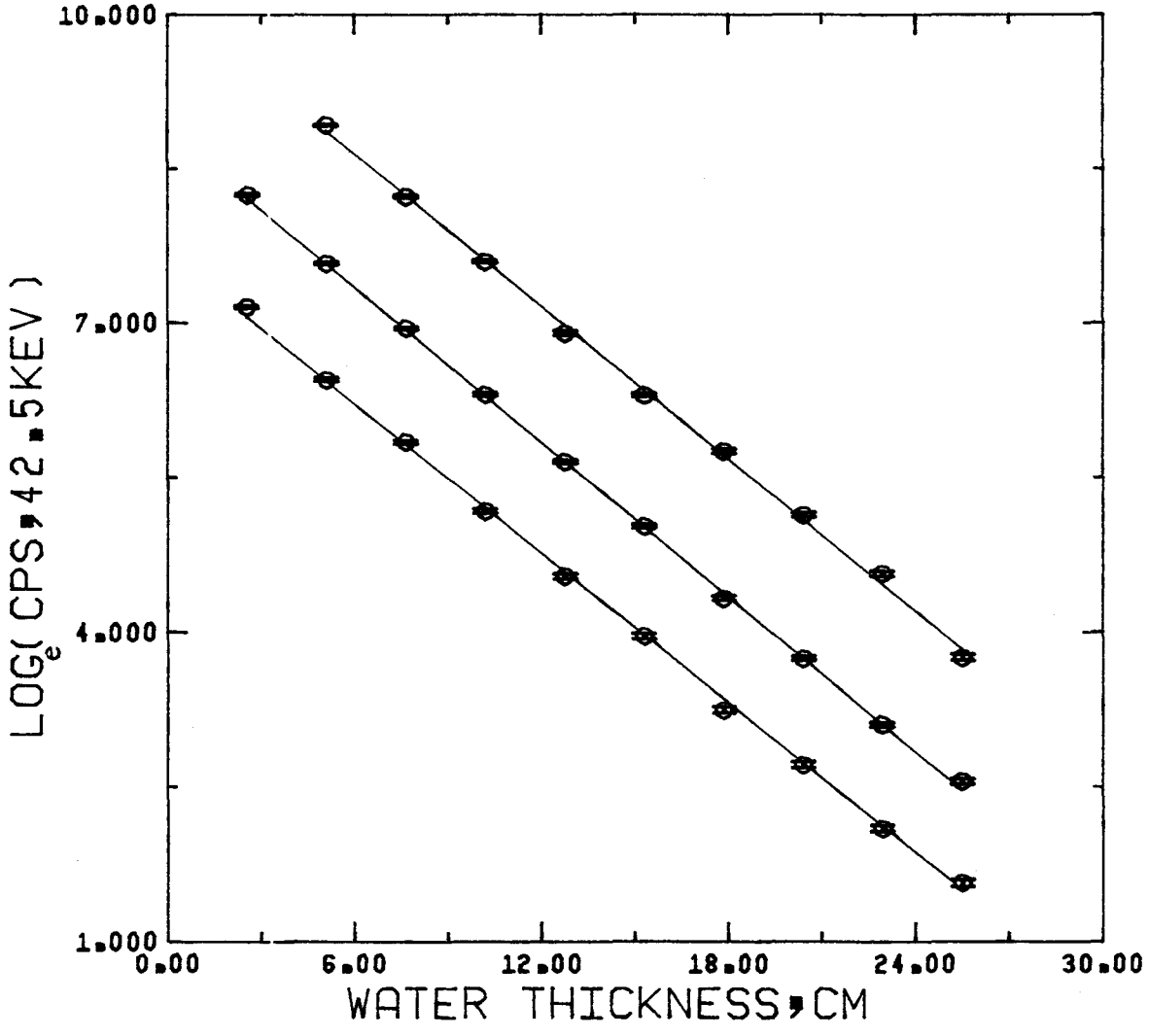

Fig. 3.2 : Transmission of 42.5 Kev photons through water

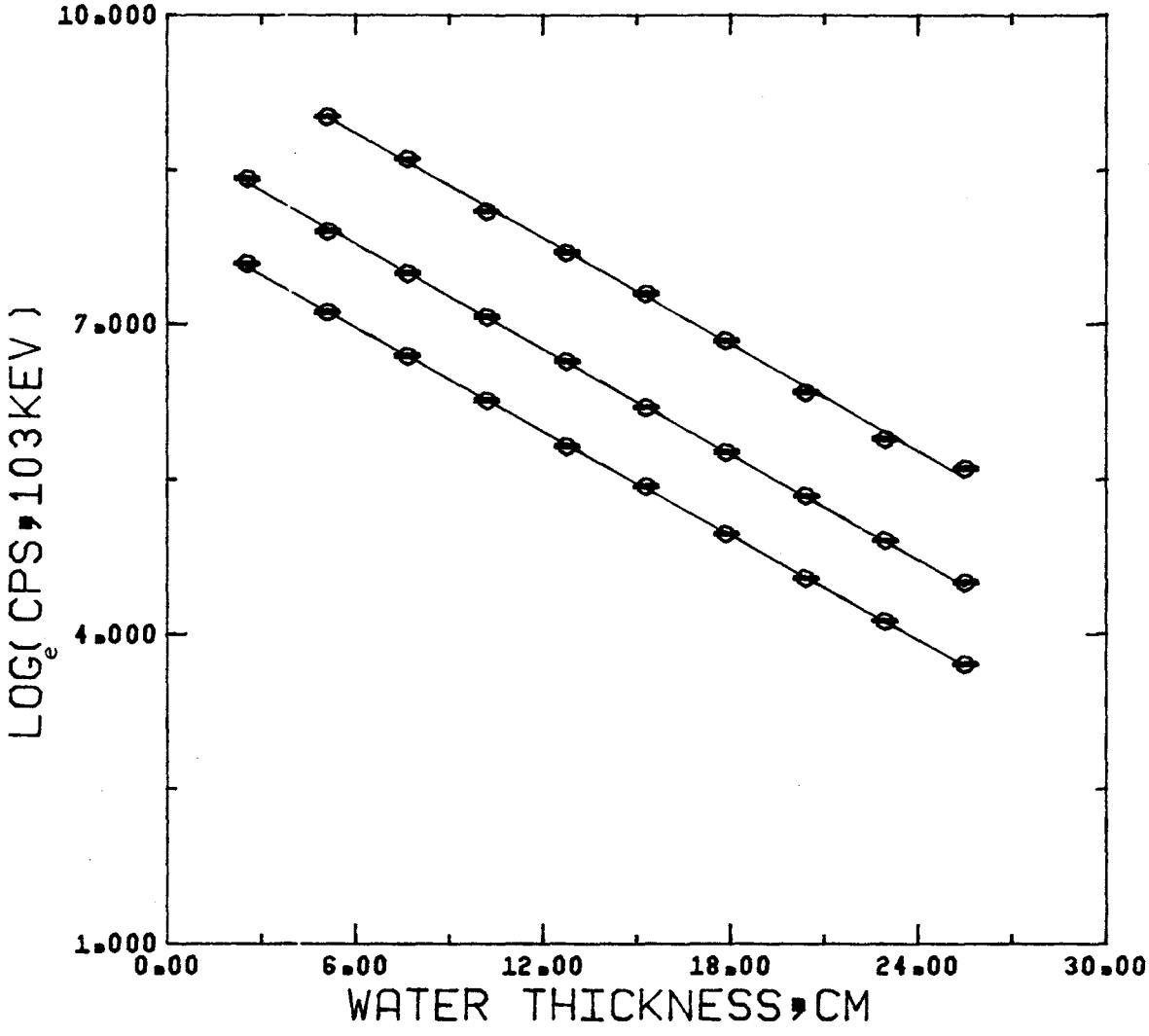

Fig.3.3 : Transmission of 103 Kev photons through water

lengthened by an input event reaching the system while the previous event is being processed. The following mathematical expressions, in which N_i and N_o are the true and observed count rates and τ is the system deadtime [30], describe the two cases.

paralyzable deadtime: $N_o = N_i\, e^{-N_i\tau}$

nonparalyzable deadtime: $N_o = \frac{N_i}{(1+N_i\tau)}$ or $N_i = \frac{N_o}{(1-N_o\tau)}$

As reported [30], it is apparent that for a paralyzable system, the observed count rate increases to a maximum and then decreases. At very high true count rates, the observed count rate becomes zero and the system is totally paralyzed. Also, two values of the true count rate (one very much greater than the other) could give rise to the same observed count rate, leading to the possibility of incorrect assessments of source activities. On the other hand, in a non-paralyzable system, the observed count rate increases asymptotically to τ^{-1} for true count rates $>>\tau^{-1}$ and the system can never be paralyzed. Hence, it is preferred to have a system with non-paralyzable deadtime.

In the dual photon measurement system, the true count rate was determined using the pulser counts registered in the MCA. At low count rates both paralyzable and nonparalyzable systems look similar. From Fig. 3.4 and 3.5 of the observed versus true count rates of the 42.5 kev and 103 kev photons, it is apparent that the count rates are in such a region. The deadtime of a system is variable; the mean was computed in the above region of count rates. Using the 103 kev count rates in Table 3.1 and the expressions for paralyzable and non-paralyzable systems, a mean value of 8.5 μsec was obtained for the

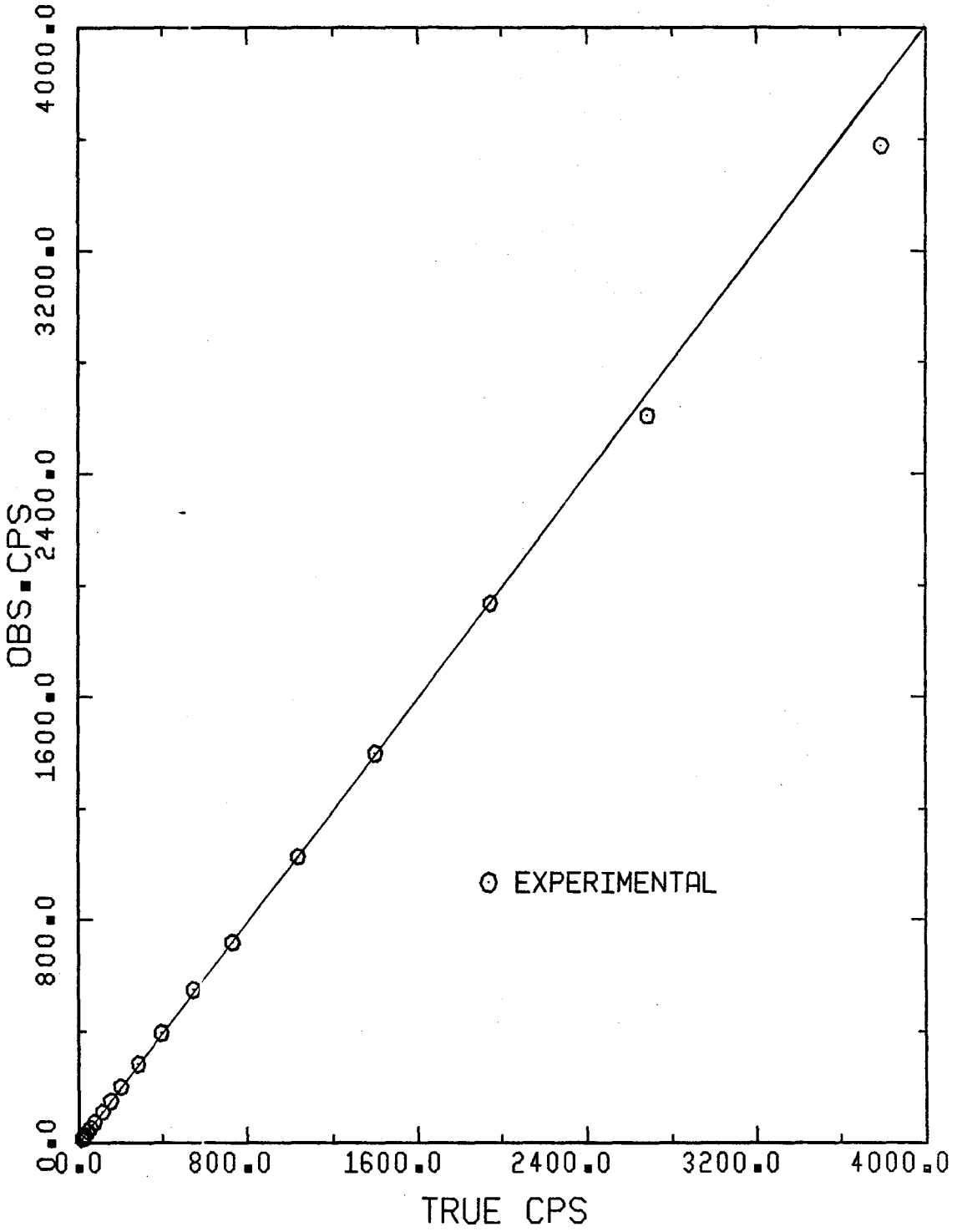

Fig. 3.4: True vs. observed CPS for 42.5 kev.

The line indicates zero deadtime losses

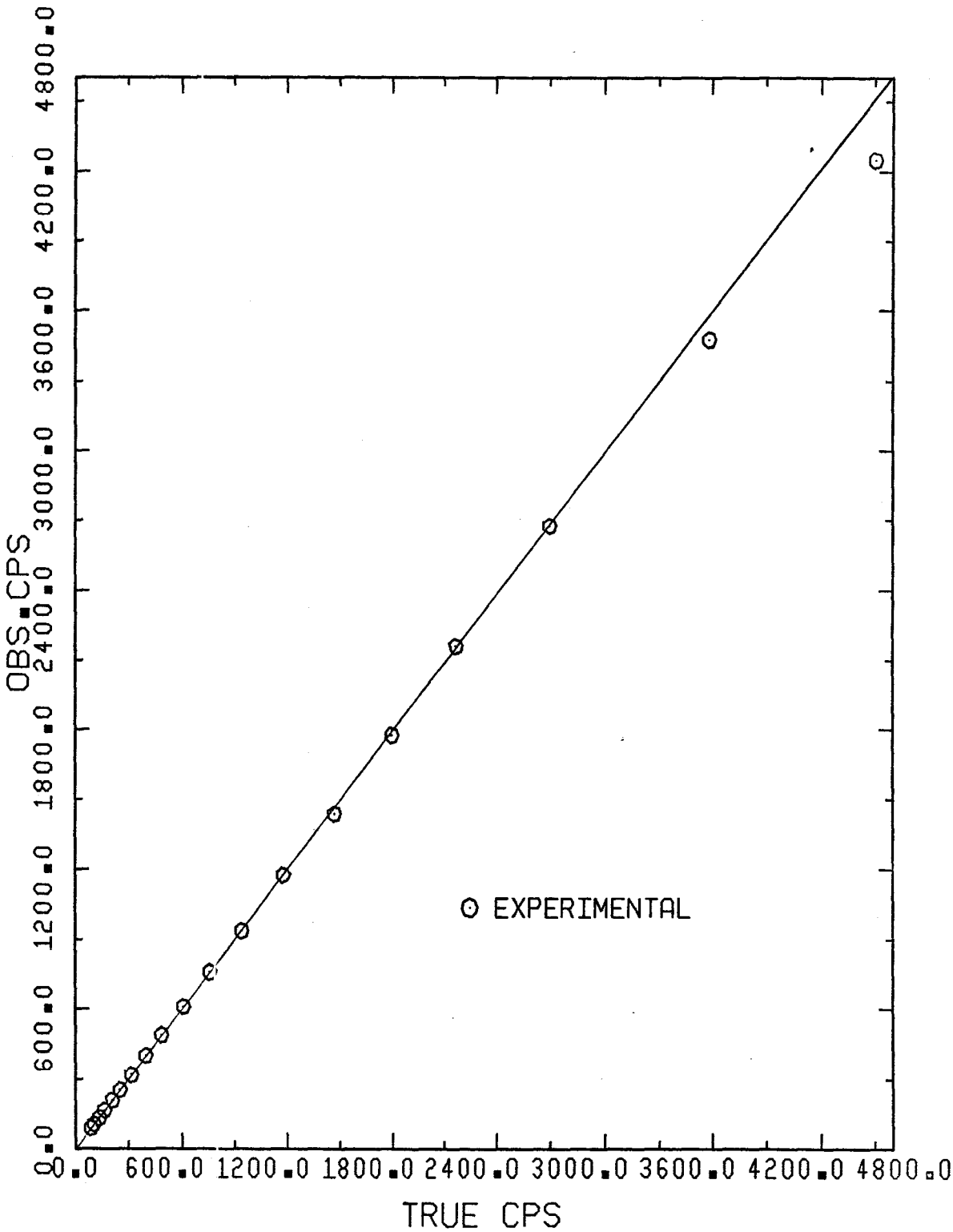

Fig. 3.5: True vs. observed CPS for 103 kev.
The line indicates zero deadtime losses

system deadtime. Since the MCA has a live time clock for deadtime correction of pulses reaching its input stage, it is concluded that the effective deadtime is restricted to that in the detector electronics. Experiments described later, have shown that a count rate less than 2000/s is adequate for DPA in phantom measurements and since the counts lost due to deadtime at this count rate is less than 1.7%, no deadtime corrections are consequently made.

3.3 Self-Absorption

The photon output of the source maybe less than that expected from its activity because of photon absorption within the source material. From the data of Storm and Israel [23], the attenuation coefficients for Sm and O were interpolated to obtain the values for Sm_2O_3 at 42.5 kev and 103 kev. The values are shown in Table 3.2. For comparison, the corresponding values for Gd have also been included to indicate the greater fraction of counts absorbed in a Gd source. The theoretical values for Sm_2O_3 attenuation coefficient at 42.5 kev and 103 kev were found to be 4.582 cm^2g^{-1} and 2.221 cm^2g^{-1} respectively. A simple experiment was performed to verify these values. The component B (in fig. 3.1) was removed from an empty graphite capsule and the resultant cavity filled tightly with non-radioactive Sm_2O_3. Count rate measurements were made with the source and detector in the configuration described in Sec. 3.1 above and with known thicknesses of water as absorber to reduce deadtime errors. In each case, counts were registered in the MCA with and without the second graphite capsule on top of the source in the source holder so that the photons were

ENERGY (KeV)	ABSORPTION COEFFICIENT $cm^2 g^{-1}$			
	Sm	O	$Sm_2 O_3$	Gd
42.5	5.293	0.080	4.582	5.725
103	2.570	0.008	2.221	2.748

TABLE 3.2 - Attenuation coefficient for $Sm_2 O_3$ and Gd

attenuated through known quantities of Sm_2O_3. The water thickness was different for each measurement so that count rates were of the same magnitude. The thickness (x) of Sm_2O_3 was given by the ratio of the mass of Sm_2O_3 inserted in the capsule and the cross sectional area within the capsule, in units of gcm^{-2}. This experiment was repeated six times to examine the reproducibility of the measurement. Table 3.3 gives the results obtained from the above experiment. From the mean of the $\exp(\mu x)$ values at 42.5 kev and 103 kev, mean values of the absorption coefficients were obtained as 4.230 cm^2g^{-1} and 2.294 cm^2g^{-1} respectively. This is in good agreement with the calculated theoretical values. The pulser counts were once again used to obtain true count rates. In a typical ^{153}Sm source used for DPA in the present study, 39.9% of photons at 42.5 kev and 16.3% of photons at 103 kev are lost due to self absorption. [34]

For a given source activity the photon output will be greatest when self absorption is minimized. The total intensity of the 42.5 kev and 103 kev photons from ^{153}Gd is given [30] as 121.6% and 21.1% respectively. From ^{153}Sm the corresponding values are 60.8% and 28.3%. The apparent advantage of ^{153}Gd over ^{153}Sm will be partially offset by the greater self-absorption in ^{153}Gd. For source masses greater than 0.7 gcm^{-2}, the 42.5 and 103 kev photon intensities are greater for ^{153}Sm than for ^{153}Gd.

3.4 Activity vs. Count Rate

During a period of about six months, five different labelled graphite capsules, each containing about 26 mg of enriched Sm_2O_3, were

Mass of Sm_2O_3 in graphite capsule = 0.4590 g

Cross sectional area within capsule = $\pi(\frac{0.635}{2})^2 = 0.3167$ cm^2

$\therefore$ Area density of Sm_2O_3, x = 1.449 g cm^{-2}

Count time in all following cases = 300 sec.

ABSORBER		42.5 KeV	103 KeV	Pulser	$\mu x/_{42.5}$	$\mu x/_{103}$
Sm_2O_3	H_2O	Counts	Counts	Counts		
Yes	50 cc	6249	171003	17967	6.139	3.325
No	300 cc	115116	552251	17300		
No	300 cc	114317	547977	17948	6.146	3.343
Yes	50 cc	6165	166975	17955		
Yes	50 cc	6212	166584	17986	6.082	3.288
No	300 cc	108120	518328	17885		
No	250 cc	199282	788110	17461	6.118	3.299
Yes	50 cc	5798	162808	17969		
Yes	50 cc	5779	161792	17983	6.157	3.339
No	250 cc	206571	815619	17758		
No	250 cc	207047	814294	17495	6.138	3.350
Yes	50 cc	5903	160254	17974		
				Mean	6.130	3.324

$\therefore$ Mean μ at 42.5 KeV = 4.230 cm^{2}g^{-1} $\pm$ 0.127

Mean μ at 103 KeV = 2.294 cm^{2}g^{-1} $\pm$ 0.057

TABLE 3.3 - Calculation of source self-absorption

irradiated for a few hours. Count rate measurements were made for the 42.5 kev and 103 kev photons. In every case the source activity was determined using a calibrated Ge(Li) spectrometer. The high energy 463.6 kev, 521.3 kev, (531.4+533.3) kev, 539.1 kev and 609.1 kev photons of ^{153}Sm were counted. The intensity data taken from [31] are shown in Table 3.4 along with the detector efficiency at these energies taken from the energy calibration curve. The observed MCA count rates of the 42.5 kev and 103 kev photons at different calculated activities are given in Table 3.5 and plotted in Fig. 3.6 and 3.7 respectively. It is quite evident from these graphs that the observed count rate varies linearly with the source activity. These results enable the use of standard ^{153}Sm sources in the dual photon method so that the activity of each source can be derived from the NaI(Tℓ) detector count rate - (with reference absorbers used to reduce deadtime errors), without having to use the Ge(Li) spectrometer each time. This also facilitates quicker and easier means of dose calculations in invivo applications. In addition, these charts would help determine the useful time period of a given source for DPA.

3.5 Beam Geometry

For stationary, intermittent and continuous scanning measurements the photon beam size at various levels in the absorber is of great importance in DPA. In all these cases narrow beam geometry is preferred in order to minimize errors due to scattering of primary photons in the absorber. The error due to beam size arises from overlapping at the boundaries of the absorber and also due to averaging of attenuation across

Absolute intensity of 103.1 KeV photons = 28.3%

ENERGY KeV	RELATIVE INTENSITY	Ge (Li)DETECTOR EFFICIENCY
103.1	100	-
463.6	0.053	3.25×10^{-4}
521.3	0.028	2.85×10^{-4}
531.4 + 533.3	0.357	2.80×10^{-4}
539.1	0.086	2.75×10^{-4}
609.1	0.051	2.425×10^{-4}

TABLE 3.4 - Energy-efficiency data for Ge (Li) Spectrometer

ACTIVITY M Ci	OBSERVED NaI CPS	
	42.5 KeV	103 KeV
22.85	11686.9	6892.8
17.81	9105.4	5310.6
12.38	6086.2	3304.2
8.59	4209.0	2315.0
4.21	1999.5	1007.0
2.98	1425.1	734.3
2.25	1234.3	621.0
1.08	861.6	442.5
0.40	325.6	184.9

TABLE 3.5 - Activity vs count rate with NaI (Tl)

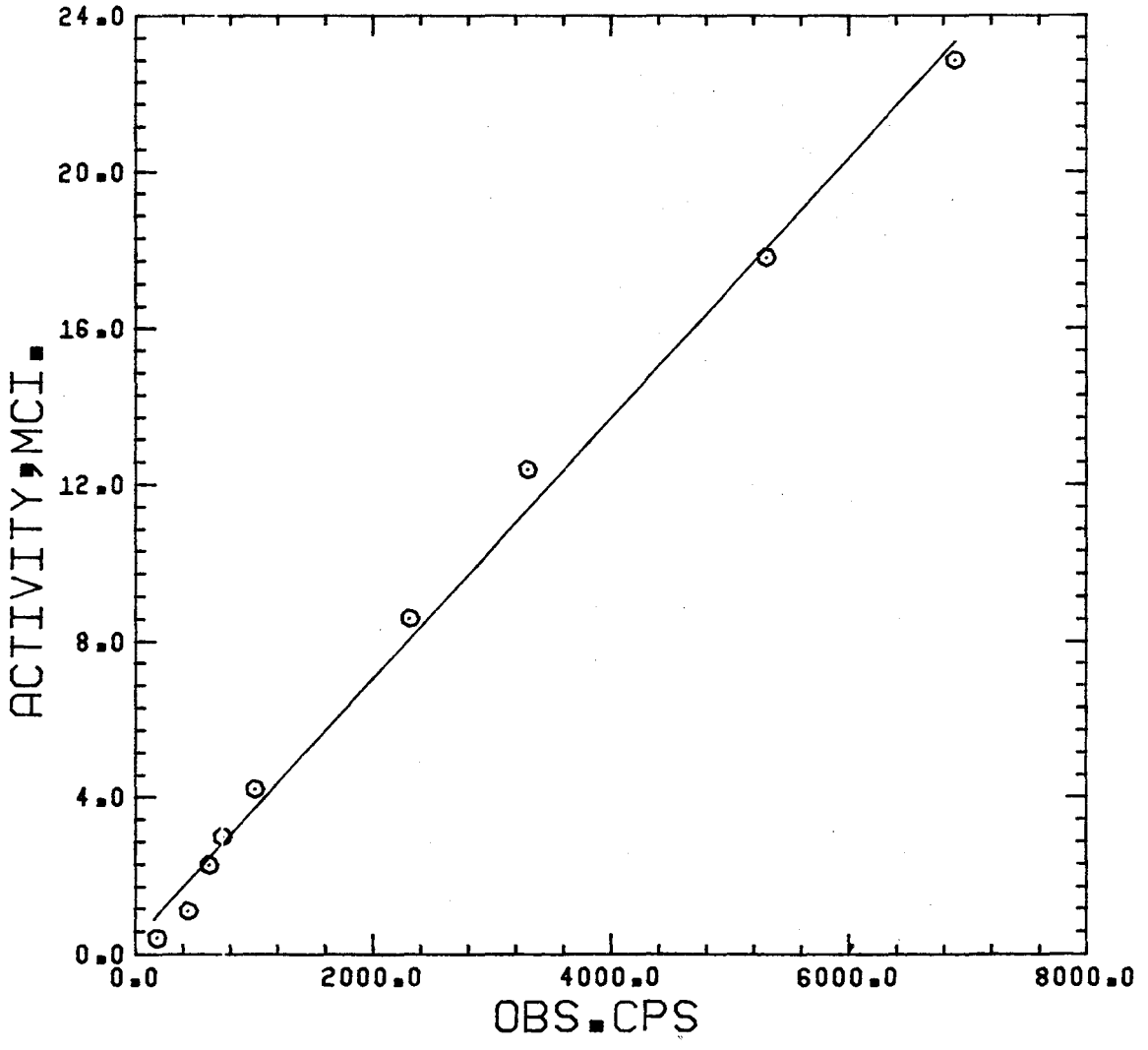

Fig. 3.6: Observed CPS vs. Activity for 42.5 kev photons.
(Y = 0.001979X - 0.0625 ; r = 0.99)

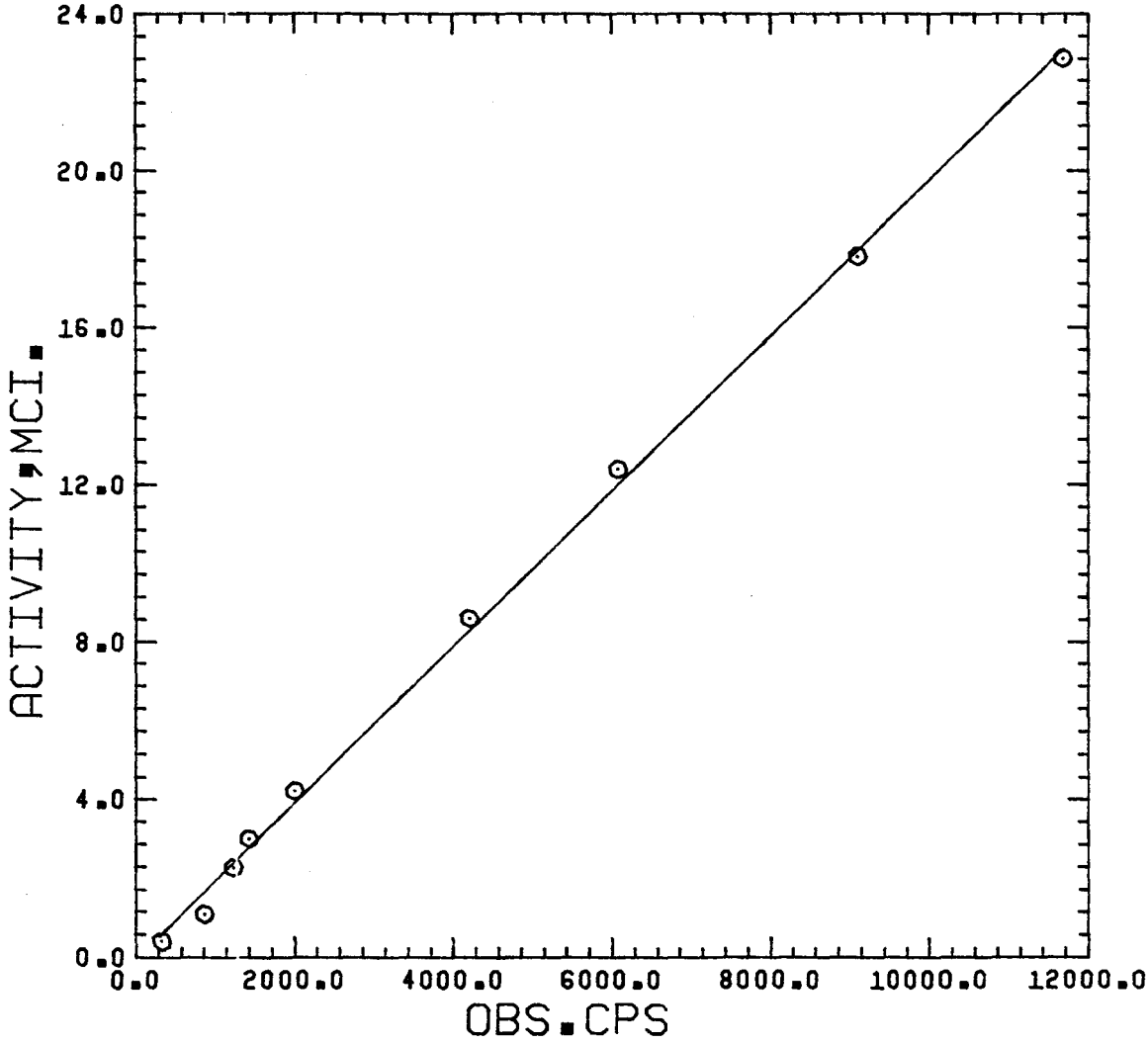

Fig. 3.7: Observed CPS vs. Activity for 103 kev photons.
(Y = 0.003334X + 0.3506 ; r = 0.99)

the beam profile. According to Watt [32], for greatest accuracy the beam diameter should be about one-third of the smallest bone width that is to be measured with a limitation imposed by counting precision. Typically, in an adult, the lumbar vertebra measures 4.0 cm long, 3.0 cm wide and 2.5 cm thick, and the transverse processes 2.0 cm long, 1.0 cm wide and 0.5 cm thick.

With the 2 mm diameter collimator the beam size at different distances from the source was determined using a strong ^{153}Sm source at the same distance from the detector (49.6 cm) as before. Photographic films were placed across the beam for a few hours at different distances from the top of the source collimator. After development of these films, the circular images obtained were scanned with a Joyce Loebel scanning microdensitometer. The beam profiles obtained are shown in fig. 3.8. The FWHM was measured in each case to represent the effective beam diameter. The results are given in Table 3.6; a linear relationship between beam diameter and distance from the source collimator face was determined as given below:

Beam Dia. [cm] = Dist. from collimator [cm] x 0.062 + 0.464

For a typical patient lying prone on the scanner table, the beam diameter at entry of the body surface is 0.59 cm and at the exit 1.83 cm. The beam diameter at the detector collimator face is 2.82 cm.

DISTANCE FROM COLLIMATOR cm.	BEAM DIAMETER cm.
5.0	0.79
8.0	0.90
12.7	1.27
17.8	1.59
24.6	2.01
36.5	2.70

TABLE 3.6 - Photon beam geometry

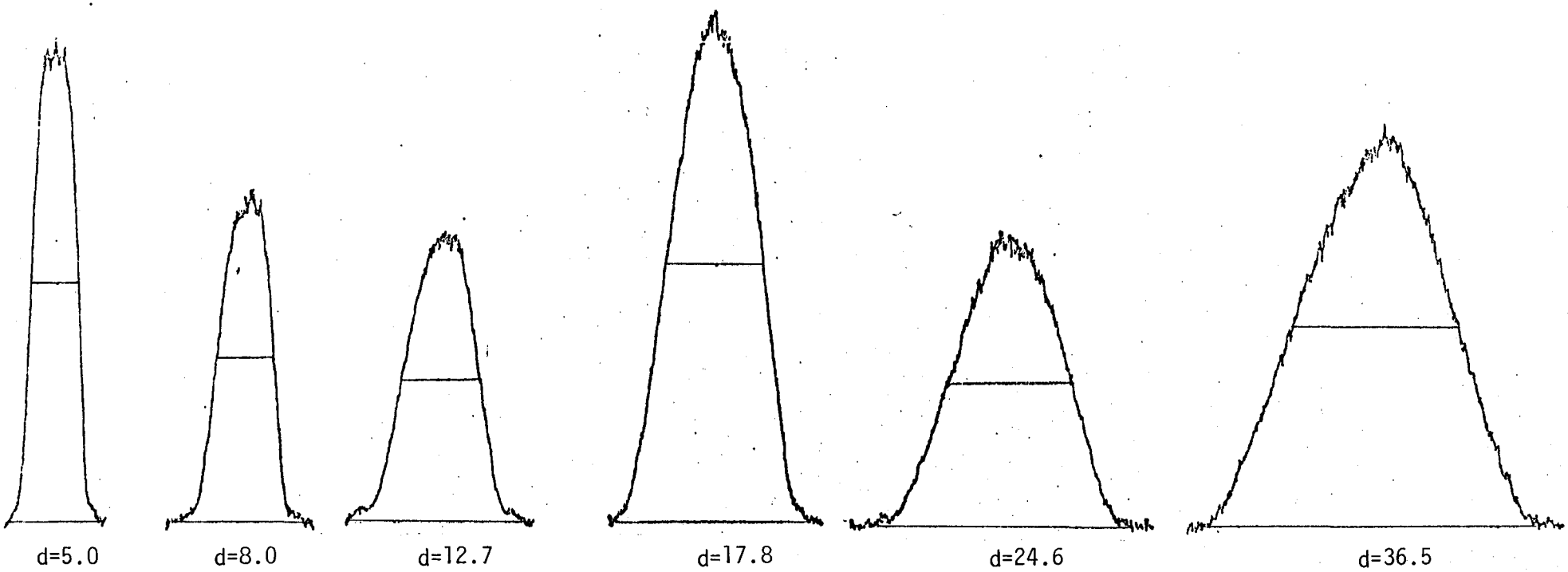

Fig. 3.8: Beam profiles at different distances from source collimator face.

d= distances in cm from source collimator face.

CHAPTER 4

Dual Photon Absorptiometry

The validity of dual photon transmission measurements of elemental mass was investigated using phantoms of known composition and size. The phantoms tested were aluminum sheets immersed in water and acrylic resin cylinders containing $Ca_3(PO_4)_2$ again submerged in water. The results obtained with the resin cylinders were compared with measurements using a commercial single photon bone densitometer.

4.1 Theory

As indicated in chapter 1, the equations for transmission of photons at two discrete energies in a two component system are [33]:

$$I = I_o e^{-(\mu_a m_a + \mu_b m_b)}$$

and

$$I' = I'_o e^{-(\mu'_a m_a + \mu'_b m_b)}$$

Eliminating m_b from these equations, the expression for m_a is given by

$$m_a = \frac{\mu'_b \ell n \frac{I_o}{I} - \mu_b \ell n \frac{I'_o}{I'}}{\mu_a \mu'_b - \mu'_a \mu_b}$$

$$= \left(\frac{\mu_b}{\mu'_b} \ell n \frac{I'}{I'_o} - \ell n \frac{I}{I_o}\right)\left(\frac{1}{\mu_a - \mu'_a \frac{\mu_b}{\mu'_b}}\right) \qquad (1)$$

The latter expression facilitates determination of fat composition

in soft tissue in subject measurements. As the fat percent is variable, the ratio $\frac{\mu}{\mu'}$ for soft tissue in a particular individual can be iterated from count rate measurements through points where bone mineral is absent. From this value and theoretical consideration of the ratio of attenuation coefficients, the fat fraction can be evaluated.

The attenuation coefficients at 42.5 kev and 103 kev for the components a (aluminum) and b (water) were interpolated from the data of Hubbell (1969). These values are as follows:

$\mu_a' = 0.5045\ cm^2g^{-1}$ at 42.5 kev and $\mu_a = 0.1683\ cm^2g^{-1}$ at 103 kev

$\mu_b' = 0.25548\ cm^2g^{-1}$ at 42.5 kev and $\mu_b = 0.16946\ cm^2g^{-1}$ at 103 kev

Substituting in equation (1),

$$m_a = (0.6633\ \ell n \frac{I^{42.5}}{I_0^{42.5}} - \ell n \frac{I^{103}}{I_0^{103}})(\frac{-1}{0.1663}) \qquad (2)$$

4.2 Absorptiometry in Aluminum

Experiments were performed with aluminum sheets suspended in water. Aluminum thicknesses of 0.1575, 0.325 and 0.65 cm were measured. For each aluminum standard three different water thicknesses were used. The water thickness varied from 7.5 cm to 20.4 cm. Measurements were made with the aluminum sheets located at different sections of the beam, at distances between 5.5 cm and 11.0 cm from the source collimator face. The beam diameter varied from 0.8 cm to 1.15 cm.

In order to reduce errors due to crossover correction and counting statistics, 30% window settings were used at both the 42.5 kev and 103 kev channels in the MCA. The crossover correction measured as

described previously was found to be 1.5% with this window setting. The results are presented in Table 4.1. In invivo measurements, patients with different soft tissue thicknesses in the lumbar region will be encountered. In the present experiment water was used analogous to soft tissue; hence different thicknesses were used in the transmission measurements to simulate the conditions of measurements on human subjects. The number of counts accumulated was such that the precision of the results varied from 1.5-4.5%. From Table 4.1 it can be seen that the accuracy varied from 0.1-3.8%. From the foregoing, it is apparent that within these limits of water thickness and beam size, beam hardening and beam geometry do not affect the results for stationary measurements. The activity of the ^{153}Sm source used in these measurements was about 85 mci and source-detector distance was 49.6 cm.

4.3 Absorptiometry Using Bone Phantoms

Bone phantoms in the form of cast acrylic resin cylinders, 25 mm diameter by 75 mm long, were measured by DPA after being immersed in water with their long axes vertical. These phantoms were made to contain concentrations of $Ca_3(PO_4)_2$ varying from 75 mg/ml to 200 mg/ml in increments of 25 mg/ml. The window settings and source-detector distance were maintained the same as with the aluminum standards. The attenuation coefficients at 42.5 kev and 103 kev for the various mixtures were determined using the elemental attenuation coefficients derived from the data of Veigele [35]; the resultant values are shown in Table 4.2.

Three repeat measurements were made for each phantom with the same ^{153}Sm source (activity = 144 mCi) during a period of two weeks.

Al cm	Beam Dia. cm	Water thk.cm with Al	Water thk.cm w/o Al	Count time Sec.	Pulser Counts with Al	Pulser Counts w/o Al	Corr.42.5 Kev CPS with Al	Corr.42.5 Kev CPS w/o Al	103 KeV CPS with Al	103 KeV CPS w/o Al	Measured Mass of Al gcm^{-2}	True Mass of Al gcm^{-2}
0.1575	0.80	13.7	9.6	300	17616	17954	290.7	952.5	1057.9	2171.6	0.409	0.425
	0.99	11.8	7.4	500	29809	29227	180.0	620.7	522.3	1109.0	0.410	
	1.15	10.3	8.8	500	29954	29755	123.1	296.8	357.7	598.4	0.416	
0.325	0.80	13.7	9.6	300	17962	17639	322.4	1231.0	1351.9	2849.5	0.860	0.877
	0.99	10.5	7.6	500	29865	29856	122.8	407.7	382.6	733.1	0.876	
	1.15	10.8	8.8	500	29901	29916	94.6	286.4	321.7	580.1	0.873	
0.65	0.80	20.4	15.3	400	23988	23984	34.5	274.8	443.4	1305.7	1.782	1.755
	0.99	20.4	12.7	300	17875	17963	34.8	529.1	438.3	1983.2	1.778	
	1.15	17.8	10.2	400	23791	23905	53.5	834.4	558.3	2556.3	1.808	

TABLE 4.1 - Dual photon transmission measurements with Al standards

PHANTOM NUMBER	CONCN. of $Ca_3(PO_4)_2$ IN THE MIXTURE $\frac{mg}{ml}$	$\mu_{42.5}$ $cm^2 g^{-1}$	μ_{103} $cm^2 g^{-1}$
2	100	.2811	.1671
3	175	.3185	.1686
5	75	.2676	.1655
6	125	.2932	.1668
7	150	.3065	.1684
8	200	.3308	.1700

TABLE 4.2 - Calculated attenuation coefficients for bone phantoms

The precision of the resultant mass densities calculated using equation (1), ranged from 1.5-3.5%. Table 4.3 shows the experimental results for the six bone phantoms.

Next, the phantoms were individually scanned on a clinical densitometer (Norland, model 278A) using a single photon source, ^{125}I(28 kev). The cylinders were immersed in 4.0 cm of water with their long axes horizontal and scanned across the diameter. The scanner computations were performed for an edge cut off value of 75%; Table 4.4 gives the observations from three repeat measurements. The mean of the values obtained by DPA (Table 4.3) and the densitometer (Table 4.4) are shown in Table 4.5 and plotted in figure 4.1. A high correlation ($r=0.97$) was observed between these values.

PHANTOM No.	BASELINE COUNTS/SEC.		ABSORBER QTY.	ABSORBER WIDTH	ABSORBER DENSITY
	Left	Right	gcm^{-1}	cm	gcm^{-2}
2	1276	1266	0.452	2.121	0.213
2	1263	1263	0.418	2.044	0.205
2	1289	1289	0.418	2.097	0.199
3	1266	1266	0.766	2.320	0.330
3	1263	1263	0.732	2.226	0.329
3	1285	1285	0.733	2.263	0.324
5	1304	1276	0.333	2.047	0.163
5	1261	1261	0.286	1.961	0.146
5	1285	1285	0.310	2.095	0.148
6	1276	1276	0.528	2.079	0.254
6	1263	1263	0.508	2.128	0.239
6	1261	1285	0.486	2.108	0.231
7	1289	1289	0.617	2.192	0.281
7	1261	1261	0.589	2.213	0.266
7	1289	1263	0.589	2.185	0.270
8	1263	1263	0.880	2.321	0.379
8	1285	1261	0.861	2.339	0.368
8	1285	1285	0.859	2.263	0.380

TABLE 4.4 - Bone phantom measurements on the clinical densitometer

ABSORBER		Count Time Sec.	42.5 KeV Counts	103 KeV Counts	Mass Density gm cm^{-2}
Water cm	Phantom No.				
12.6	-	40	22625	114483	
12.6	5	40	10424	71342	3.42
12.6	5	40	9941	69534	3.91
12.6	5	40	10017	69361	3.28
12.6	-	40	34247	95852	
12.6	7	40	16419	74713	6.83
12.6	7	40	16493	74440	6.64
12.6	7	40	16890	75410	6.56
11.5	-	20	37109	105034	
12.1	8	20	11136	72829	8.75
11.5	-	20	33111	94916	
12.6	8	20	8911	60349	8.45
12.6	-	30	33050	101292	
12.6	8	30	11572	76347	8.36
12.6	-	40	34247	95852	
12.6	3	40	14152	75655	8.19
12.6	3	40	13998	75009	8.16
12.6	3	40	13729	74680	8.35
11.5	-	20	32208	101126	
12.1	2	20	13644	62463	4.54
11.5	-	20	30316	99042	
12.6	2	20	12765	61428	4.96
12.6	-	30	29850	96423	
12.6	2	30	12984	60746	4.65
12.6	-	40	34247	95852	
12.6	6	40	19807	79259	6.25
12.6	6	40	19347	77929	6.20
11.5	-	20	37109	105034	
12.6	6	20	18526	79116	6.41

TABLE 4.3 - Dual photon transmission measurements with bone phantoms

Phantom No.	From DPA gcm^{-2}	From Densitometer gcm^{-2}
2	4.71	0.206
3	8.23	0.328
5	3.53	0.152
6	6.28	0.241
7	6.67	0.272
8	8.52	0.376

TABLE 4.5 - Comparison of results from DPA and the clinical densitometer

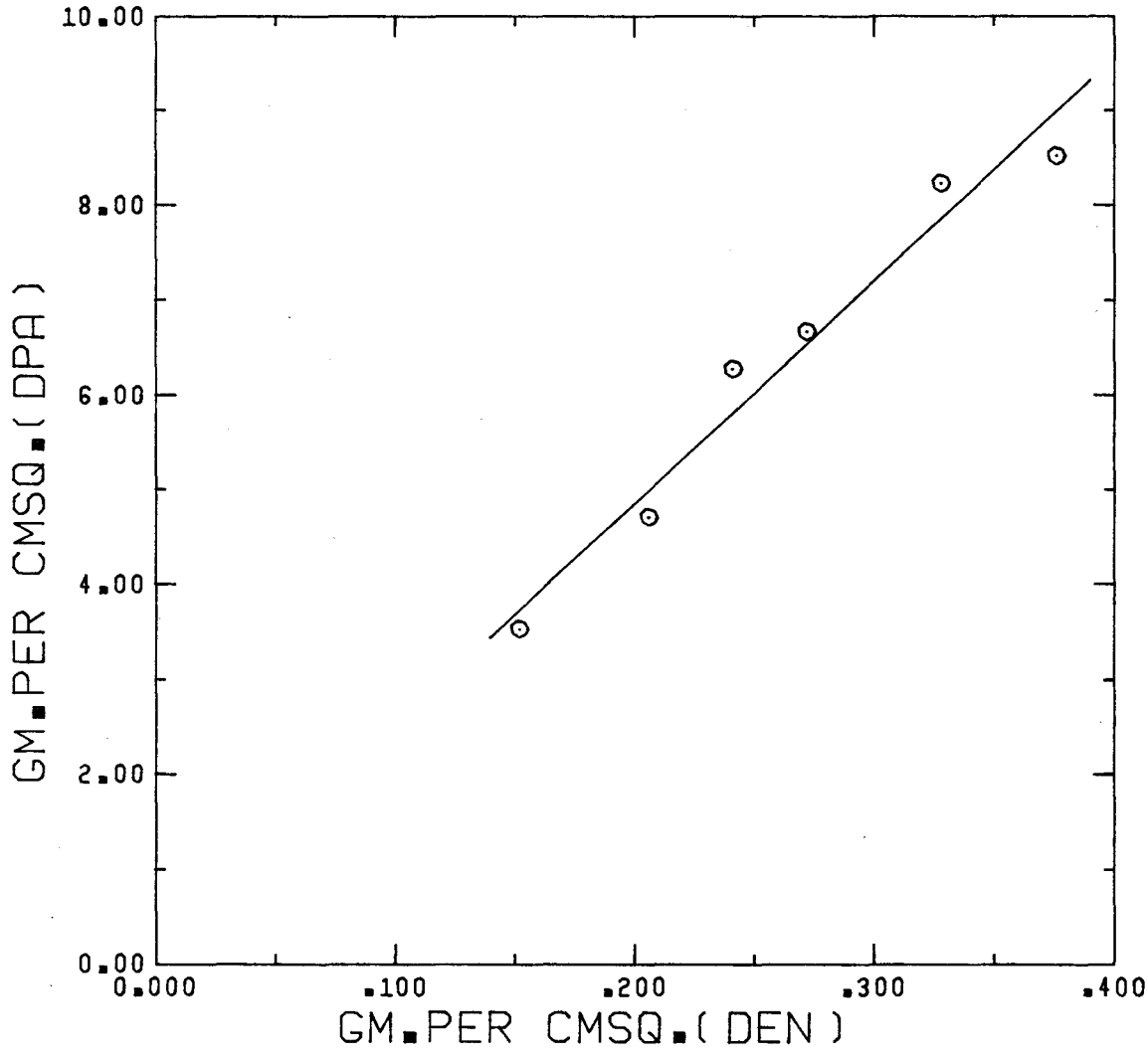

Fig.4.1 : Densitometer vs. DPA measurements

(Y = 23.492X + 0.156 ; r = 0.97)

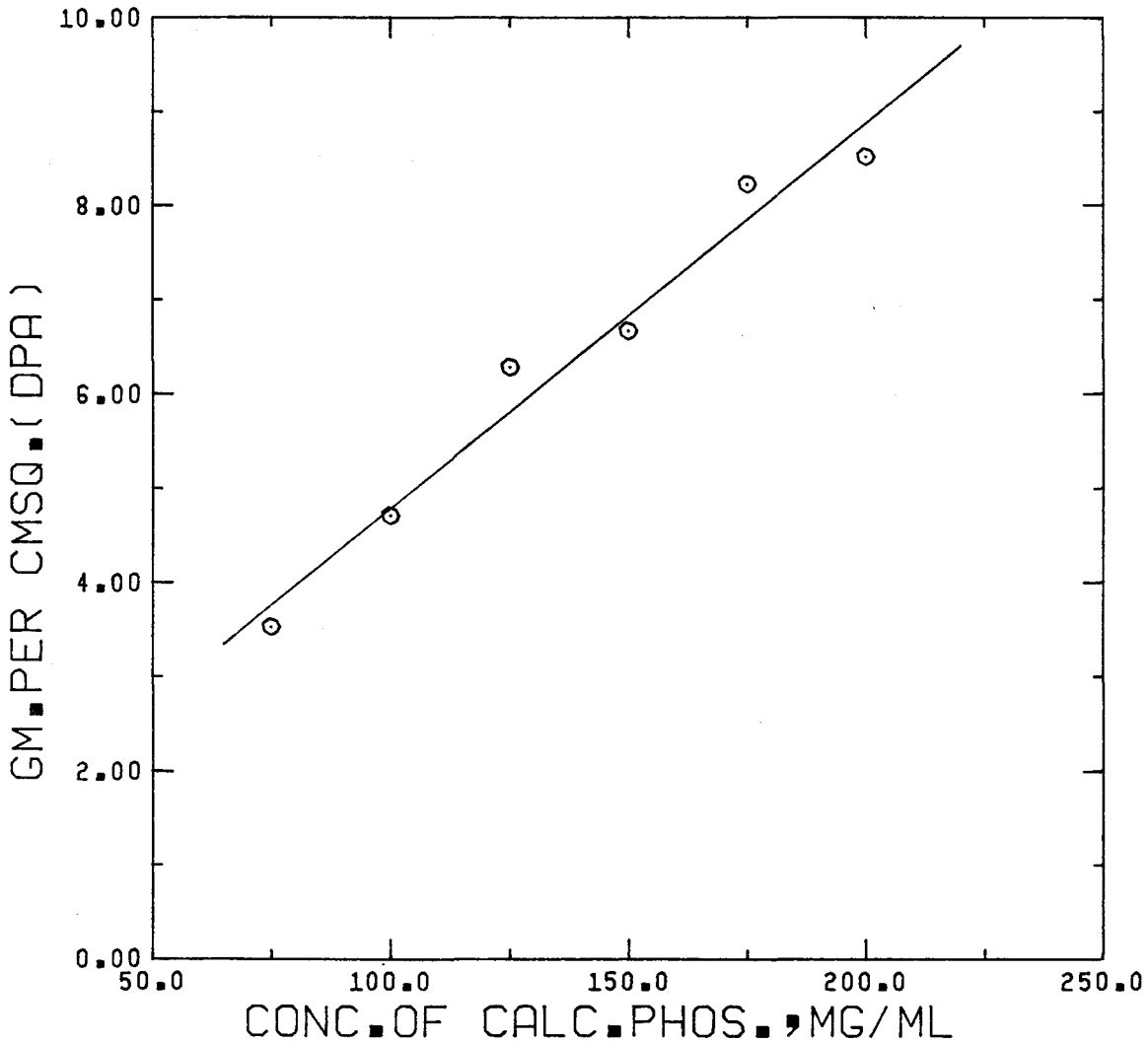

Fig.4.2 : DPA results vs.calc.phos.conc.in phantoms

(Y = 0.041X + 0.682 ; r = 0.98)

CHAPTER 5

Conclusions and Suggestions for Further Work

In this work the effectiveness of ^{153}Sm as a photon source for DPA was evaluated. This preliminary study has resulted in useful conclusions regarding this source, making way for further invitro and invivo measurements on lumbar vertebrae to proceed.

The 42.5 kev and 103 kev photons of ^{153}Sm were found to obey the exponential law of attenuation and thus the fundamental principle of the method is satisfied. The errors due to deadtime were less than 1.7% and hence deadtime correction was not very significant. However, for sources of the order of 1.0 Ci, the deadtime errors would be very high when no absorbers are present. Hence, to determine count rates in air with such sources, known thicknesses of standard absorbers have to be used. In DPA the percentage deadtime error has to be examined with a typical absorber. Self absorption in the samarium source used in DPA was calculated. It was found that 39.9% of the low energy and 16.3% of the high energy photons were absorbed in the source itself. The detector efficiency at 42.5 kev and 103 kev was determined as 0.90 and 0.71 respectively. Considering this and the high percentage loss of photons due to self-absorption in the source, it is suggested that in order to obtain greater count rates (and consequently greater precision) the length of the graphite insert (B in fig. 3.1) be reduced and the capsule irradiated for a longer time. For a desired count rate, the charts of activity vs. count rate can be used to determine the

irradiation time required for a particular source. From the derived photon beam geometry and results of Watt [32], it is concluded that the 2 mm diameter source collimator is suitable for DPA of the lumbar vertebrae.

The dual photon method yielded a precision error of 4.5% and an accuracy error up to 4% in measurements on aluminum standards and bone phantoms immersed in water. These results prove the usefulness of ^{153}Sm for stationary point measurements by DPA.

In order to measure bone mineral content in the lumbar vertebrae, the femoral neck or the whole body, a rectilinear scan procedure is required. Dunn et al [14] modified an OHIO Nuclear rectilinear scanner for this purpose. They retained the patient table, C-frame and the drive system. The lower detector was replaced by a source holder with a beam shutter and a collimator and the upper detector by a collimated NaI(Tℓ) detector. The longitudinal movement was controlled by a constant speed stepping motor and the transverse movement by a variable speed stepping motor. Both these motors and the beam shutter were activated by computer generated signals. The positional coordinates of the source-detector system were relayed to the computer by high-resolution potentiometers coupled to the motors. As the transverse speed should be uniform over the measurement period, the true speed obtained from the positional information and elapsed time was compared with the input desired speed fed into the computer in order to indicate any deviations. The output from the lower energy in the pulse height analyser was shown on a CRT screen to aid in initial positioning and locating bone edges.

Provided the above modifications were made on our existing scanner the following measurement procedure could be followed for BMC determination. In the first instance, invitro measurements may be performed with the lumbar vertebrae (after removal from a cadaver) immersed in water. The region to be scanned may be descretized into a series of points at one second intervals along each transverse scan path. The scan velocity and scan interval would be set according to the exposure rate and source activity (typically 1.0 ci) to allow for a sufficiently large number of counts to be accumulated during each one second interval in the scan path. For automatic scanning and on-line computation of BMC, the arrangement shown in fig. 5.1 is suggested. The starting and end points of the scan path are predetermined by limit switches on the scanner console. A single control unit may be used to activate the scan start and stop, the beam shutter (on a rack and pinion arrangement) to open and close and the scalers to start and stop accumulation of counts (en route to buffers) in the two energy channels. The buffers are interfaced to a computer and the recorded counts are used for calculation of BMC in each one second interval of the scan path. By means of the potentiometers, the positional information can be transmitted to the computer through ADC's so that the calculated BMC values may be correlated.

The average value of $\frac{\mu}{\mu_T}$ defined by equation (1) in Section 4.1 is to be estimated by scanning over regions where bone mineral is absent. This value is subsequently used in the equation to calculate bone mineral mass, m_b, for each accumulated pair of counts. However, in measurements on individuals, this will lead to the determination of

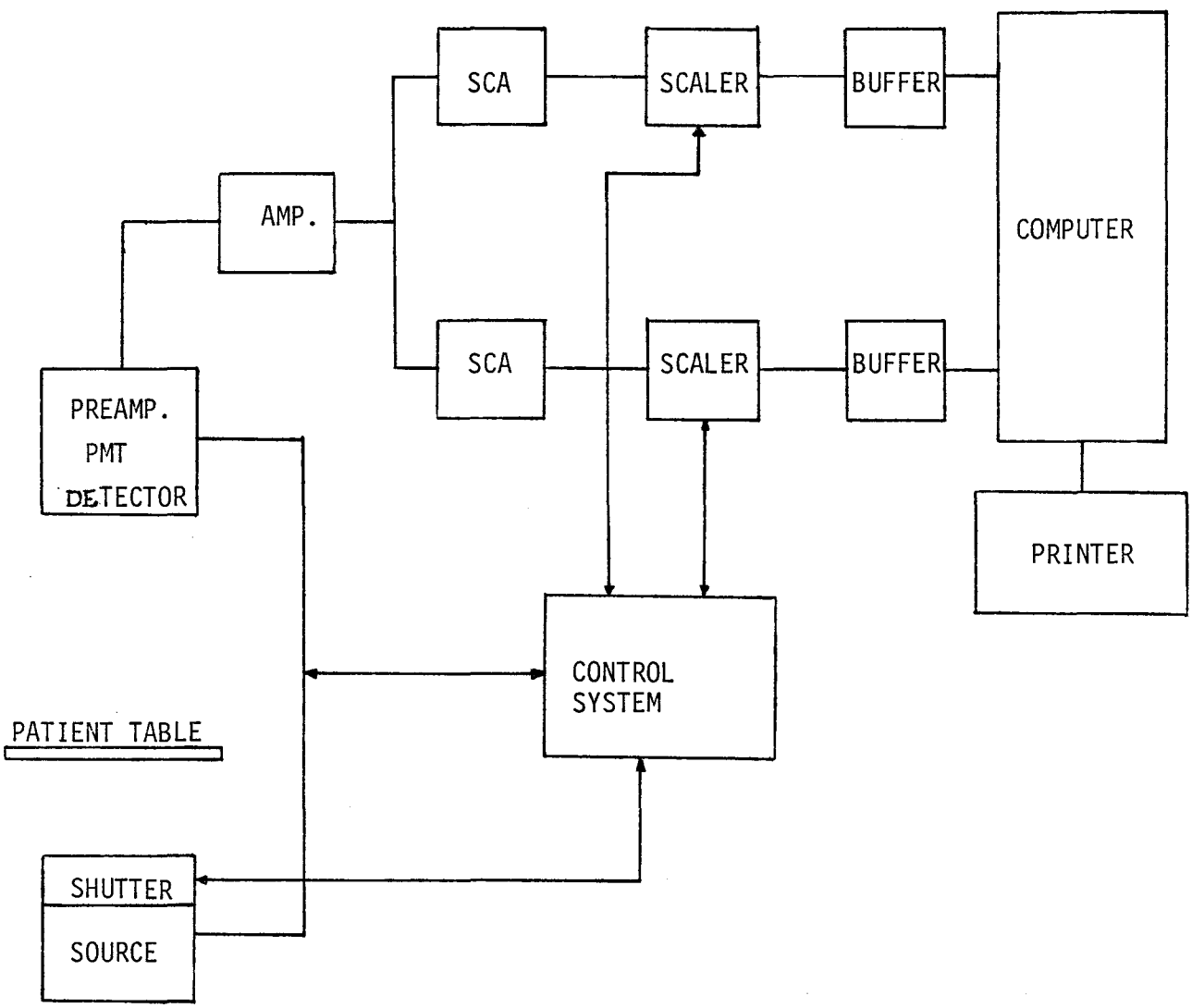

Fig. 5.1: Block diagram showing arrangement for automatic scanning.

percent fat in soft tissue. The average value of $\frac{\mu}{\mu_T}$ is computed by iteration of measurements over areas where bone mineral is absent and this value used to calculate m_b. From the mean value of $\frac{\mu}{\mu_T}$ and the linear relation between $\frac{\mu}{\mu_T}$ and fat fraction, the percent fat in soft tissue is obtained. The individual values of m_b are summed over the entire scanned region to give the total BMC. The bone width and bone edge of the individual vertebrae may be specified from calibrated cut-off values of m_b at the edges. The density distribution of bone mineral mass can be shown on a CRT screen after intensity modulation.

Before setting on to invivo measurements with human subjects, it is recommended that the radiation dose to points close to the lumbar region in a typical DPA scan be determined using TLD's fixed on an anthropomorphic model. The dose to the skin, ovaries and testicles due to a 1.0 Ci ^{153}Gd source was measured by Mazess et al [12] and was found to be 2.0, 0.09 and 0.03 mrad respectively in a lumbar spine measurement involving 10 transverse scans over the patient.

The dose to any point on the skin in a typical lumbar scan was calculated for a source strength of 1.0 Ci and scan speed of 5 mm/sec and was found to be about 0.017 mGy. Table 5.2 shows the results of the computation using the following:

$$\dot{D} = \frac{Se^{-\mu r}}{4\pi r^2} \times E \times 1.6 \times 10^{-10} \times \left(\frac{\mu_{en}}{\rho}\right)_{muscle} \text{ in mGy sec}^{-1}$$

where $\dot{D}$ is dose rate, S is no. of photons/sec., E is photon energy in MeV, $\frac{\mu_{en}}{\rho}$ is mass-energy absorption coefficient and r (=9.3 cm) is distance from the source.

kev	$(\frac{\mu_{en}}{\rho})_{muscle}$ cm^2g^{-1}	m Gy sec^{-1}
40.9	0.0701	0.0027
41.5	0.0660	0.0047
47.0	0.0572	0.0016
69.6	0.0296	0.0006
75.4	0.0280	0.00002
83.4	0.0263	0.00002
89.5	0.0260	0.00002
97.4	0.0257	0.0001
103.2	0.0256	0.0041
	Total =	0.01386

Scanning speed = 5mm/sec

Beam dia. at entrance to body = 6 mm

$\therefore$ Total dose at any point = 0.01386 x 1.2

$\tilde{}$ 0.017 mGy

Table 5.1: Calculation of dose due to a DPA scan

References

1. Griffiths, H.J., Zimmerman, R.E., An overview of clinical applications of photon absorptiometry, Am. j. Roent. Rad. Ther. Nucl. Med., 126, 1301, 1976.

2. Bartley, M.H. et al., The relationship of bone strength and bone quantity in health, disease and aging, J. of Geront., 21, 517, 1966.

3. Krolner, B., Pors Nielsen, S., Bone mineral content of the lumbar spine in normal and osteoporotic women: cross-sectional and longitudinal studies, Clinical Science, 62, 329, 1982.

4. Vose, G.P. et al., Quantitative bone strength measurements in senile osteoporosis, J. of Geront., 16, 120, 1961.

5. Cameron, J.R., Sorenson, J.A., Measurement of bone mineral invivo: an improved method, Science, 142, 230, 1963.

6. Reed, G.W., The assessment of bone mineralization from the relative transmission of ^{241}Am and ^{137}Cs radiations, Phys. Med. Biol., 11, 174, 1966.

7. Roos, B., Rosengren, B., Skoldborn, H., Determination of bone mineral content in lumbar vertebrae by a double gamma ray technique, Proc. Bone measurement conf. Chicago, 1970, CONF700515.

8. Mazess R.B. et al., Absorptiometric bone mineral determination using ^{153}Gd, Proc. Bone measurement conf. Chicago, 1970 CONF700515.

9. Hanson, J., Analysis of ^{153}Gd and of $^{125}I/^{241}Am$ sources, Proc. Int. Conf. Bone Mineral Meas., Chicago, Illinois 1973.

10. Watt, D.E., Optimum photon energies for the measurement of bone mineral and fat fractions, Br. j. Radiology, 48, 265, 1975.

11. Smith, M.A. et al., Comparison between ^{153}Gd and ^{241}Am, ^{137}Cs for dual photon absorptiometry of the spine, Phys. Med. Biol. 28, 709, 1983.

12. Mazess, R.B., et al., Progress in dual photon absorptiometry of bone, Proc. Symp. Bone Mineral Determ., Stockholm-Studsvik 1974, AE-489, Vol. 2, p. 40.

13. Wilson, C.R., Madsen, M., Dichromatic absorptiometry of vertebral bone mineral content, Invest. Radiol. 12, 180, 1977.

14. Dunn, W.L. et al., Measurement of BMC in human vertebrae and hips by dual photon absorptiometry, Radiology 136, 485, 1980.

15. Krolner, B., Pors Nielsen, S., Measurement of BMC of the lumbar spine I. Theory and application of a new two-dimensional dual photon attenuation method, Scand. j. clin. Lab. Invest. 40, 653, 1980.

16. Kan, W.C. et al., Direct readout of BMC with dichromatic absorptiometry, Proc. Int. conf. Bone mineral Meas. Chicago, Illinois, 1973.

17. Roos, B., Skoldborn, H., Dual photon absorptiometry in lumbar vertebrae I. Theory and Methods, Acta Radiologica, Ther. Phys. Biol. 13, 266, 1974.

18. Condon, B. et al., Dual photon densitometry of the lumbar spine, Calc. Tiss. Int. 27s, A8, 1979.

19. Tothill, P. et al., Dual photon absorptiometry for the determination of bone mineral in the lumbar spine, calc. Tiss. Int. 33s, 185, 1981.

20. Riggs, B.L. et al., Differential changes in bone mineral density of the appendicular and axial skeleton with aging, J. Clin. Invest. 67, 328, 1981.

21. Davis, M.W., Webber, C.E., The reactor production of a low energy, high intensity photon beam, Nucl. Instr. Meth., 154, 395, 1978.

22. Rieppo, R., Face type NaI detector efficiencies for low energy γ-rays, Int. j. app. rad. isot. 27, 491, 1976.

23. Storm, E., Israel, H., Photon CS from 1 kev to 100 Mev for elements z=1 to z=100, Nuclear Data Tables A7, 565, 1970.

24. Hubbell, J.H., Photon CS, attenuation coefficients and energy absorption coefficients from 10 kev to 100 Gev, NSRDS-NBS29, U.S. Dept. of Commerce, 1969.

25. Avignone, F.T. III, Jeffreys, J.A., Polynomial fits for NaI absorption coefficients, Nucl. Instr. Meth. 179, 159, 1981.

26. Lederer, C.M., et al., Table of Isotopes, John Wiley and Sons Inc., 6th Ed., 1967.

27. Gamma ray energy tables for NAA, Report No. WSUNRC-97(2), Nuclear Radiation Center, Washington, 1970.

28. Legrand, J. et al., Table de Radio Nucleides, commissariat à l'energie atomique, LMRI, 1975.

29. Schötzig, U. et al., Standardization and decay data of ^{133}Ba, Int. j. app. rad. isot. 28, 503, 1977.

30. NCRP Report No. 58, A handbook of radioactivity measurements procedures, Washington, D.C., Nov. 1978, p. 55-66.

31. Heath, R.L., Gamma-ray spectrum catalogue, Ge(Li) and Si(Li) spectrometry, ANCR-1000-2, U.S. Dept. of Commerce, Springfield, VA, 3rd ed., Vol. 2 of 2.

32. Watt, D.E. and Logan, R., Photon beam energy and size effects in the measurement of linear bone mineral mass, Proc. Symp. on bone mineral determinations, Aktiebolaget Atomenergi, Studsvik, Sweden, 1974, p. 149-165.

33. Peppler, W.W., Mazess, R.B., Total body bone mineral and lean body mass by DPA, I. Theory and measurement procedure, Calc. Tiss. Int. 33, 353, 1981.

34. Reactor Shielding Design Manual,USAEC,Ed.by T.Rockwell 1956,p.364.

35. Wm. J. Veigele,Photon C.S.from 0.1 to 1 Mev for elements z=1 to z=94, Atomic Data Tables 5, 51, 1973.